NASA TECHNICAL NOTE

NASA TN D-7941

DEVELOPMENT OF A REMOTE DIGITAL
AUGMENTATION SYSTEM AND APPLICATION
TO A REMOTELY PILOTED RESEARCH VEHICLE

John W. Edwards and Dwain A. Deets

Flight Research Center
Edwards, Calif. 93523

1. Report No. NASA TN D-7941	2. Government Accession No	3. Recipient's Catalog No.	
4. Title and Subtitle DEVELOPMENT OF A REMOTE DIGITAL AUGMENTATION SYSTEM AND APPLICATION TO A REMOTELY PILOTED RESEARCH VEHICLE		5. Report Date	
		6. Performing Organization Code	
7. Author(s) John W. Edwards and Dwain A. Deets		8. Performing Organization Report No. H-854	
9. Performing Organization Name and Address NASA Flight Research Center P. O. Box 273 Edwards, California 93523		10. Work Unit No. 760-67-05	
		11. Contract or Grant No.	
12. Sponsoring Agency Name and Address National Aeronautics and Space Administration Washington, D. C. 20546		13. Type of Report and Period Covered Technical Note	
		14. Sponsoring Agency Code	

16. Abstract

A cost-effective approach to flight testing advanced control concepts with remotely piloted vehicles is described. The approach utilizes a ground-based digital computer coupled to the remotely piloted vehicle's motion sensors and control surface actuators through telemetry links to provide high bandwidth feedback control. The application of the system to the control of an unmanned 3/8-scale model of the F-15 airplane is described. The model was flown by a ground-based pilot from the remotely piloted research vehicle facility at the NASA Flight Research Center. The model was remotely augmented; that is, the F-15 mechanical and control augmentation flight control systems were simulated by the ground-based computer, rather than being in the vehicle itself. The results of flight tests of the model at high angles of attack are discussed.

17. Key Words (Suggested by Author(s)) Control systems Remotely piloted vehicle Digital flight control	18. Distribution Statement Unclassified - Unlimited Category: 05		
19. Security Classif. (of this report) Unclassified	20. Security Classif. (of this page) Unclassified	21. No. of Pages 52	22. Price* $4.25

DEVELOPMENT OF A REMOTE DIGITAL AUGMENTATION SYSTEM AND

APPLICATION TO A REMOTELY PILOTED RESEARCH VEHICLE

John W. Edwards and Dwain A. Deets
Flight Research Center

INTRODUCTION

The NASA Flight Research Center has developed a facility for flight testing aircraft using a remotely piloted research vehicle (RPRV) technique. This technique involves a pilot who controls the flight-test vehicle from a ground-based cockpit, and a ground-based digital computer for computation of command signals. The remote pilot cockpit and the computer are coupled to the flight-test vehicle through telemetry uplink and downlink data channels. This concept evolved from an interest in developing a low-cost alternative to full-scale manned prototype testing for high-risk flight tests such as stalls and spins.

The flight-test capability of the NASA Flight Research Center's RPRV facility is enhanced by its remotely augmented vehicle (RAV) system, which can provide remote augmentation for manned or unmanned test vehicles. In this system the ground-based digital computer provides closed-loop control law computation for the remote vehicle. The closed-loop control laws can be implemented on the computer by using FORTRAN programing, which removes much of the complexity from the onboard systems. The computer can simulate either digital flight control systems or analog flight control systems. The RAV system is not suitable for duplicating some flight control concepts such as redundancy management or multiple channel operation.

The RPRV technique was used at the NASA Flight Research Center in a flight-test program on a 3/8-scale model of the F-15 airplane. The RPRV systems used in this research program were checked out on a PA-30 airplane (ref. 1). The development of the RPRV testing technique is summarized in reference 2. The objective of the scale-model flight-test program was to investigate the high-angle-of-attack stall-spin region of the F-15 airplane. For this program the RAV system simulated the full-scale F-15 analog control system (both the open-loop mechanical control system and the closed-loop control augmentation system). It also provided basic control modes that enabled stability and control data to be obtained from the flight data.

This report describes the RPRV facility at the NASA Flight Research Center, the development of the digital RAV system, and its application to the scale-model F-15 flight-test program.

SYMBOLS

a	model scale factor
$a_i, b_i, c_i, d_i, \alpha_i, \beta_i$	coordinates of poles and zeros of general s-plane transfer function
b, c, d, β	coordinates of specific poles and zeros in s-plane transfer function
C^*	longitudinal performance index, $n_z - \dfrac{V_{co}}{g} q$
$F_{\delta_e}, F_{\delta_a}$	longitudinal and lateral stick force, respectively, N
$G(\cdot)$	general transfer function where $(\cdot)$ is (s), (w), or (z)
$G_0(s)$	zero-order hold transfer function
g	acceleration of gravity, m/sec^2
I	moment of inertia, N/m^2
I_X	moment of inertia about X-axis, kg-m^2
I_{XZ}	product of inertia, kg-m^2
I_Y	moment of inertia about Y-axis, kg-m^2
I_Z	moment of inertia about Z-axis, kg-m^2
i	index variable
$j = \sqrt{-1}$	
$K_{(\cdot)}$	feedback gain associated with $(\cdot)$
K', K''	general filter gain constants
k	difference between order of numerator and denominator of $G(s)$
l	length, m
M	Mach number
$M_\alpha, M_q, M_{\delta_e}, Z_\alpha, Z_{\delta_e}$	dimensionalized stability and control derivatives for longitudinal short-period equations of motion

2

m	mass, kg
n,t	number of complex pairs of roots in numerator and denominator, respectively, of general transfer function
n_z, n_y	airplane normal and lateral acceleration, respectively, g
Δn_z	incremental change in airplane normal acceleration, g
p,q,r	airplane roll, pitch, and yaw rate, respectively, deg/sec
$Re\ z, Im\ z$	abscissa and ordinate of z-plane, respectively
s	s-plane complex variable
T	sample period, sec
u,r	number of real roots in numerator and denominator, respectively, of general transfer function
V	velocity, m/sec
V_c	speed of sound, m/sec
V_{co}	crossover velocity for C^* index, m/sec
w	w-plane complex variable, $\dfrac{z-1}{z+1}$
z	z-plane complex variable, e^{sT}
α, β	angle of attack and angle of sideslip, respectively, deg
δ_a	aileron signal, $\frac{1}{2}\left(\delta_{a_L} - \delta_{a_R}\right)$, deg
$\delta_{a_L}, \delta_{a_R}$	left and right aileron position, respectively, positive trailing edge down, deg
δ_{a_p}	pilot's lateral stick position, cm
δ_a / δ_{a_p}	lateral stick gearing ratio, deg/cm
δ_d	differential stabilator signal, $\frac{1}{2}\left(\delta_{h_L} - \delta_{h_R}\right)$, deg

$\delta_{d_{CAS}}$ contribution to δ_d from roll command augmentation system, deg

$\delta_{d_{MCS}}$ contribution to δ_d from roll mechanical control system, deg

δ_{e_p} pilot's longitudinal stick position, cm

$\delta_{e_{trim}}, \delta_{a_{trim}}, \delta_{r_{trim}}$ longitudinal, lateral, and yaw trim, respectively, cm

δ_h collective stabilator signal, $\frac{1}{2}\left(\delta_{h_L} + \delta_{h_R}\right)$, deg

$\delta_{h_{CAS}}$ pitch command augmentation system command, deg

$\delta_{h_L}, \delta_{h_R}$ left and right stabilator position, respectively, positive trailing edge down, deg

δ_{pb} pitch boost servo output, deg

δ'_{pb} lagged pitch boost servo output, deg

δ_r rudder position, deg

δ_{r_a} rudder command due to aileron interconnect, deg

δ_r / δ_{a_p} aileron-to-rudder interconnect gain, deg/cm

δ_{r_p} pilot's rudder pedal position, cm

$\delta_1, \delta_2, \delta_3, \delta_4$ general uplink commands of RPRV system, counts

ζ damping ratio

θ pitch angle, deg

$\ddot{\theta}$ angular acceleration, deg/sec^2

μ, η abscissa and ordinate of w-plane, respectively

ν kinematic viscosity, m^2/sec

ρ atmospheric density, kg/m^3

σ, ε	abscissa and ordinate of s-plane, respectively
ω	frequency, rad/sec

Subscripts:

c	commanded variable
f	full scale
max	maximum value
s	stability axis
sp	short period

Abbreviations:

CAS	control augmentation system
MCS	mechanical control system

REMOTELY PILOTED RESEARCH VEHICLE FACILITY

A block diagram of the RPRV system is shown in figure 1. The vehicle response variables are telemetered to a ground station where they are routed to a ground computer, a ground cockpit instrument panel, and analog strip chart recorders for real-time flight monitoring. The ground cockpit proportional control functions (longitudinal and lateral stick and rudder pedals) are processed by the analog-to-digital converter and are trunked to the ground computer together with the mode panel signals. The ground computer calculates the command variables and provides them to the uplink encoder. Figure 2 shows the location of the components of the RPRV system in the RPRV facility. The ground cockpit (not shown) is adjacent to the cockpit electronics racks, which makes the RPRV system a self-contained, dedicated facility except for the uplink and downlink transmission and reception systems.

The RPRV system uses two uplink encoders (fig. 1). The computer encoder receives command variables from the computer, and the bypass encoder receives command variables directly from the ground cockpit. The RPRV pilot selects an encoder by means of a pushbutton on the mode control panel. The bypass encoder serves as a backup to the computer encoder if the computer malfunctions. The command signals are transmitted to the test vehicle, where they are decoded and sent to the appropriate servochannel.

The pilot may select one of two telemetry uplink antennas: an antenna slaved to a radar tracking antenna, or a fixed antenna. The uplink antennas and the uplink encoders are the only dualized components in the RPRV system. Since the system is intended for flight research, it was designed as a single channel system except for the critical uplink channel.
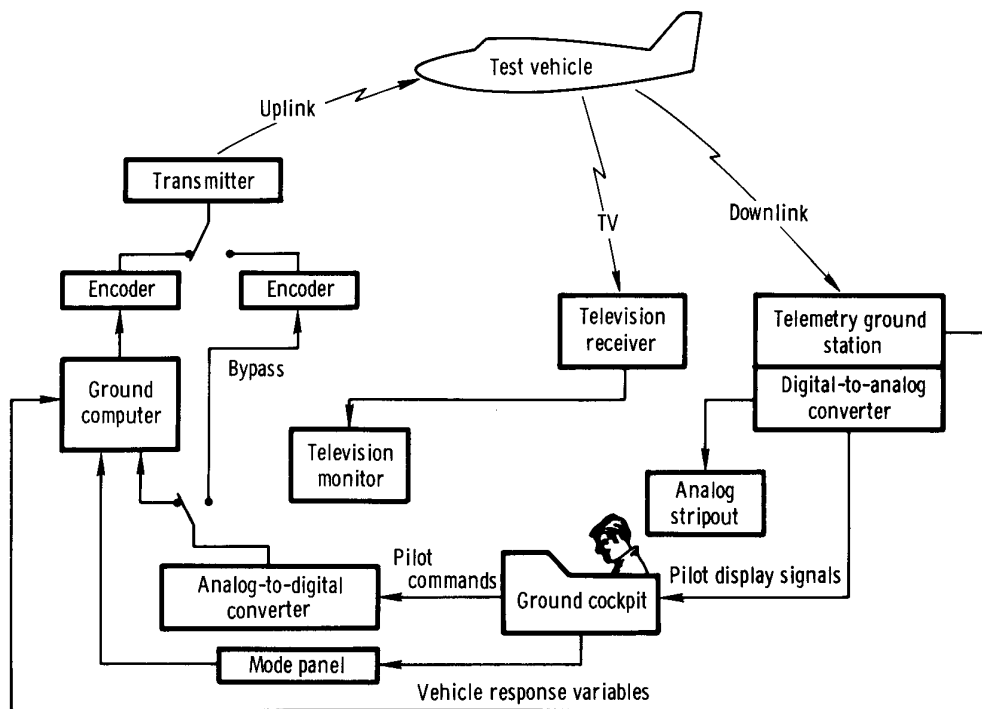
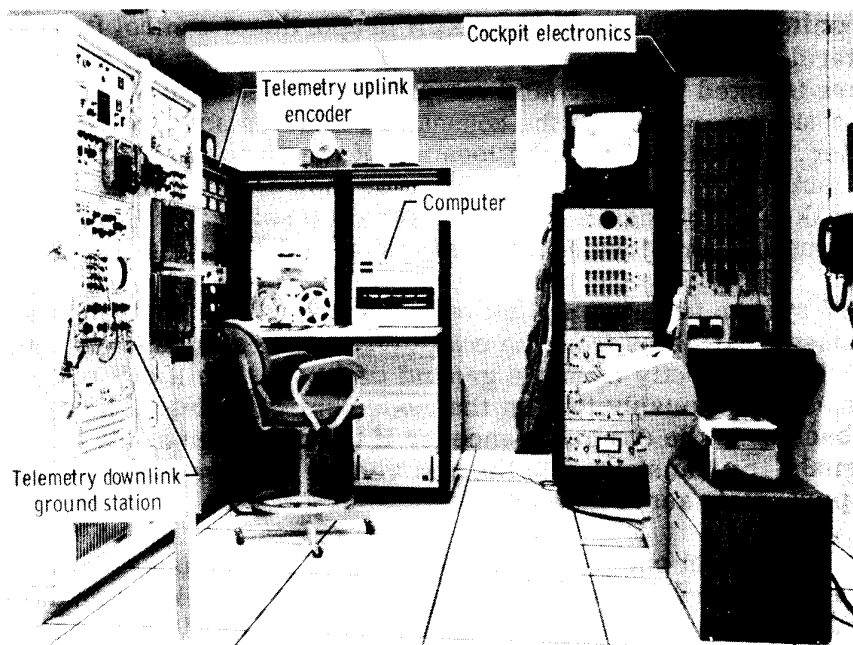Figure 1. Functional block diagram of the RPRV system.

Figure 2. RPRV facility equipment.   E-26105

Ground Cockpit

In the operation of the RPRV system, the remote pilot is given direct proportional control of the test vehicle. This makes it possible to use experienced test pilots so that the maximum research capability can be realized from the system. Accordingly, the ground cockpit is configured to provide the pilot with as much information as possible about the test vehicle and with complete control over the system. Figure 3 is a photograph of the ground cockpit showing the instrument panel, control stick, mode control panel, and pulse panel. The pilot controls the vehicle with a control stick and rudder pedals. The stick and pedals are part of an artificial feel system, and position limits and force gradients are adjustable. The pilot may select various control modes and gains on the mode control panel and apply control surface steps or doublets, under computer control, through the pulse panel. The mode control panel implements four control modes in three axes (pitch, roll, and yaw) and provides gain switches that can be programed in each axis. The panel also permits the pilot to select the bypass mode or computer modes and informs him if any downlink variable fails a window check. The mode control panel pushbutton switches are rear-lighted under computer control and indicate the control mode of the computer.
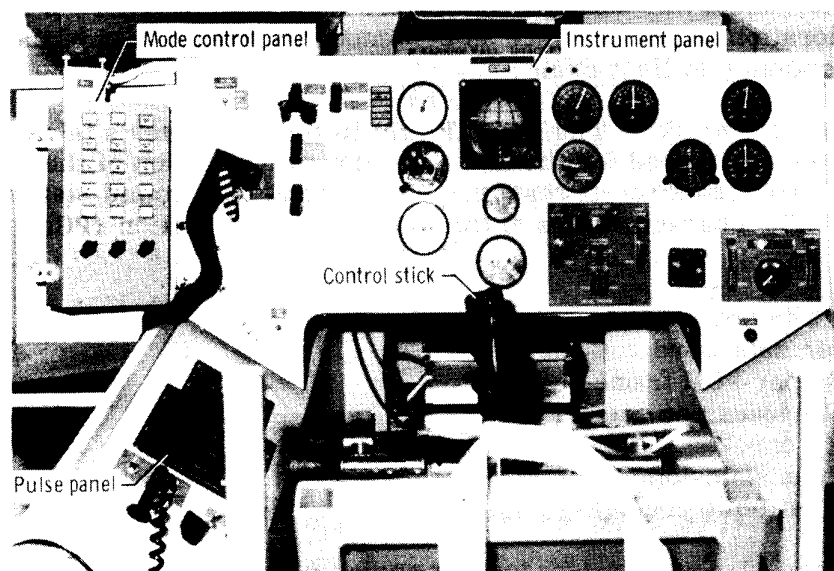

Figure 3. Remote pilot cockpit.   *E-26991*

Telemetry Downlink and Uplink

Successful operation of the telemetry data links is critical to the RPRV/RAV system. The links must be highly reliable and not introduce unacceptable time delays. During operation in a closed-loop RAV system mode, transmission losses lasting more than several tenths of a second would be unacceptable. This is in contrast to typical

7

remotely piloted drone military missions which involve the transmission of discrete commands to onboard analog autopilots and are capable of operating in hostile environments.

The time delay of the data links in the RPRV system is approximately 3.3 microseconds per kilometer, which yields a total time delay of approximately 0.5 millisecond through the downlink and uplink when the test vehicle is at a range of 75 kilometers. This is an acceptable time delay, compared to the total computational delay through the RAV system.

The telemetry links are essentially line-of-sight transmission paths, so the signal may be blocked by the wing of the test vehicle at extreme attitudes or by the horizon if the vehicle is at too low an altitude at extreme range. Thus the range of RPRV testing is a function of vehicle attitude and altitude. It was estimated that flight operations would be limited to approximately 55 kilometers at 1500 meters altitude and to approximately 185 kilometers at 13,700 meters altitude.

The number of bits in the downlink and uplink telemetry channels (9 bits in the downlink and 10 bits in the uplink) was chosen to permit valid implementation of typical closed-loop aircraft control laws. Simulator studies indicated that little increased performance was achieved with more than 10 bits, whereas less than 9 bits led to deterioration in performance as evidenced by granularity of the command signals and a tendency to limit cycle.

Telemetry downlink.— The NASA Flight Research Center's telemetry flight data acquisition system is used for the telemetry downlink portion of the RPRV system. This system provides aircraft response variables to the ground station at 200 samples per second. The characteristics of this pulse code modulation (PCM) system are as follows:

144,000 bits per second
9 bits per data word
80 words per PCM frame
200 PCM frames per second
No parity check
L-band transmission
12-foot parabolic receiving antenna slaved to radar tracking antenna

The system has 40-hertz first-order-lag analog prefilters on all channels. The low power (5 watts) and the lack of parity check on the downlink indicated the need for reasonability checks in the software to discriminate against incorrect telemetry data. The downlink is commonly used to obtain data at ranges as great as 320 kilometers for high-altitude aircraft.

Telemetry uplink.— The telemetry uplink used for the system was developed by the U.S. Navy for the remote control of drone aircraft. The system is capable of several modes of operation, from the control of a single drone to the time-multiplexed control of a fleet of drones. Because it can control more than one drone simultaneously, the update rate of the system when controlling a single aircraft is comfortably

8

high. Consequently, the system has good research capability. The characteristics of the system are as follows:

16 bits per data frame (10-bit proportional command signal and 6 discrete signals)
4 data frames per cycle
53.33 cycles per second
2 parity checks per data frame
Synchronization and parity checks on each cycle
UHF band transmission
Frequency shift keying

The telemetry uplink cycle (fig. 4) consists of 4 data words (frames) and a sync word transmitted at 53.33 samples per second (18.75 milliseconds cycle time). The transfer of each data word from encoder to receiver output on board the test airplane requires 3.75 milliseconds. The four command signals are coded in the 10 most significant bits of the uplink words, with the remaining 6 bits being available for discrete signals to the test vehicle. Since parity checks are performed on each data word, intermittent dropout of the telemetry uplink signal was not expected to cause serious problems.
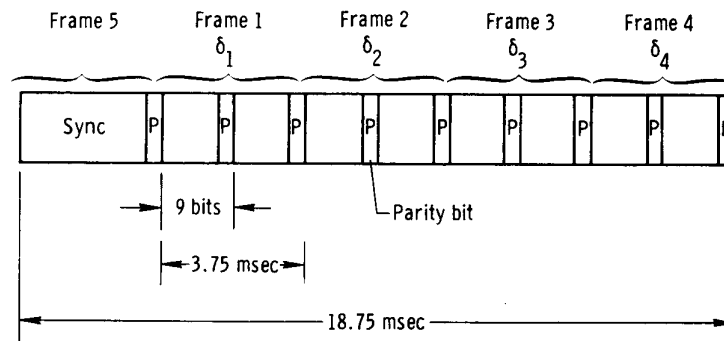
Frame 5   Frame 1   Frame 2   Frame 3   Frame 4
           δ_1 δ_2 δ_3 δ_4

| Sync | P | | P | | P | | P | | P | | P | | P | | P | | P |

9 bits

Parity bit

3.75 msec

18.75 msec

Figure 4. Telemetry uplink time schedule.

Ground Computer

The computer used in the RPRV system is a general purpose rack-mounted minicomputer with a 16K memory consisting of 16-bit words and with a 750-nanosecond cycle time. The peripheral equipment includes a card reader, line printer, magnetic tape unit, disc unit, teletype, paper tape reader/punch, and peripheral floating point processor. The software is composed of an assembler, a FORTRAN compiler, and a mathematical subroutine support library. During real-time RPRV operation, data inputs to the computer (cockpit data and downlink data) and data outputs from the computer (uplink commands) are initiated by means of input/output interrupts.

The peripheral floating point processor receives and transmits data associated with the hardware floating point operation over the input/output bus by means of the priority memory access unit. Although this operation consumes the major portion of

the 75-microsecond hardware floating point execution time, it is faster than the computer's software floating point option. It is slower, though, than may be achieved with integrated floating point hardware. A floating point data word requires two memory locations and has an 8-bit exponent and a 22-bit mantissa (six-place accuracy).

The open-loop and closed-loop control law computations are implemented through an RPRV computer program which uses floating point FORTRAN. Thus the FORTRAN compiler is used to debug and check out programs, and the floating point feature eliminates the need for variable scaling. The obvious advantage of this mode of programing in a research environment is the ease with which programs may be written and modified by a control systems engineer. The RPRV computer program also contains the assembly language subroutines which perform all input and output of data, pass the data to the FORTRAN main program, and receive the uplink command signals from the main program.

As an indication of the capability of the RPRV computer to perform feedback control law computations, approximately 0.7 millisecond is required to sum two feedback variables and a pilot command signal (each multiplied by a gain) and to operate on the resulting error signal with a first-order digital filter.

Ground Computer Input/Output Interface

Figure 5 illustrates the RPRV system interface at the computer. The number of bits in the data words passed to and from the computer is indicated in the arrows. All input/output of data is performed by assembly language interrupt servicing subroutines. The FORTRAN main program tests for the occurrence of interrupts by calls to the assembly language subroutines. The data are transferred between the assembly language routines and the FORTRAN program through the common data block and subroutine calling lists.
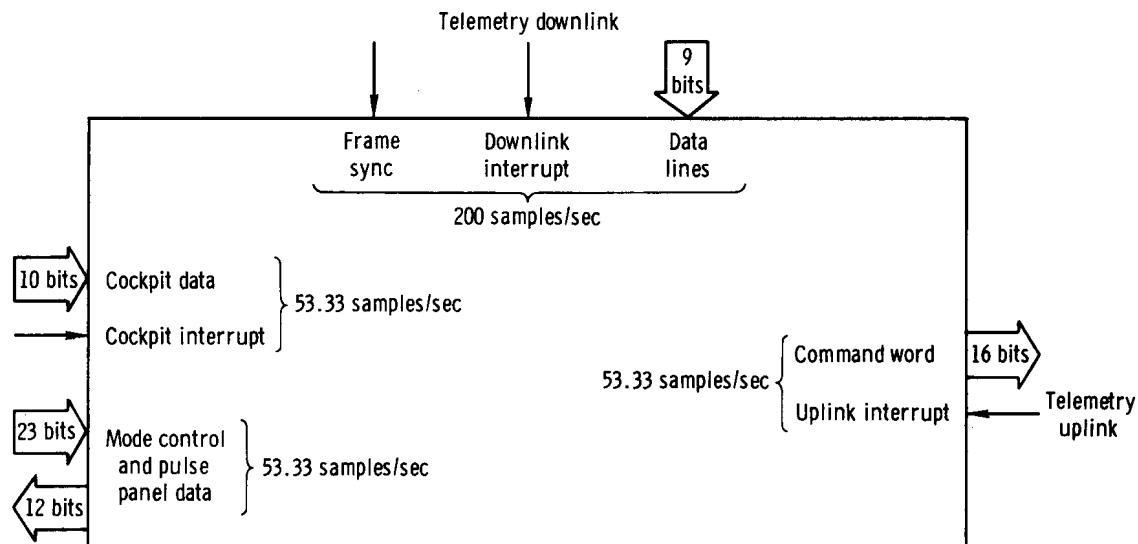

Figure 5. Input/output interface at the RPRV computer.

10

Telemetry downlink interface.— Downlink telemetry data are transferred to the computer by the downlink interrupt servicing routine at 200 samples per second for each variable. The program recognizes the variables by their sequence with respect to the FRAME SYNC PULSE which occurs once every PCM frame. The values of the variables are represented by a 0 to 511 decimal count format.

During on-line operation, the downlink interrupt servicing routine continuously updates the table of telemetry data. When the FORTRAN main program accesses the data, a window check is performed on the most recent data word to discriminate against bad data caused by loss of the downlink signal. If this word is within ±70 counts of the last "good" data word, it is accepted as valid.

Telemetry uplink interface.— The computer encoder interrupts the computer every 3.75 milliseconds to request one of the five 16-bit command words. The uplink interrupt servicing routine tests five sense lines to determine the correct variable to output. If the computer program and the uplink encoder should get out of synchronization, the computer sends the variable that the encoder requests, even though it may have anticipated sending a different variable.

Ground cockpit interface.— The pilot's proportional command signals and the mode control panel status are sampled by the computer once each cycle at a rate of 53.33 samples per second. The present mode control panel status is interrogated by the FORTRAN main program to determine if a mode change is being commanded by the pilot.

Timing and Synchronization of RPRV System

Figure 6 shows the time sequence of operations of the RPRV system. The FORTRAN program computation sequence is controlled by the uplink interrupt. For instance, during frame 1 the program computes the command signal δ_1. This command is passed to the uplink interrupt servicing subroutine, and the FORTRAN program then waits in an idle loop for an uplink interrupt. When the interrupt occurs, the FORTRAN program determines if δ_1 was requested and, if so, begins computing the next command signal, δ_2. If any other command was requested, the FORTRAN program branches to the appropriate frame in an attempt to get back into synchronization.

During frame 5, the FORTRAN program accepts the cockpit data, determines the mode control panel status, and performs mode switching initialization. The final function during frame 5 is a check to determine if the cockpit is in the bypass mode. If it is, the FORTRAN program continually loops in frame 5 awaiting the pilot's selection of a computer mode.

The downlink system is asynchronous with respect to the uplink system. The PCM data are provided at 200 samples per second, and the uplink commands are updated at 53.33 samples per second. The high data rate of the downlink system is used to minimize the time delay through the closed-loop system; all telemetry data

11

are accepted but only the most recent value of a downlink variable is used. Thus the effective overall sample rate of the flight control system is that of the system with the lowest sample rate, in this instance, the uplink system.
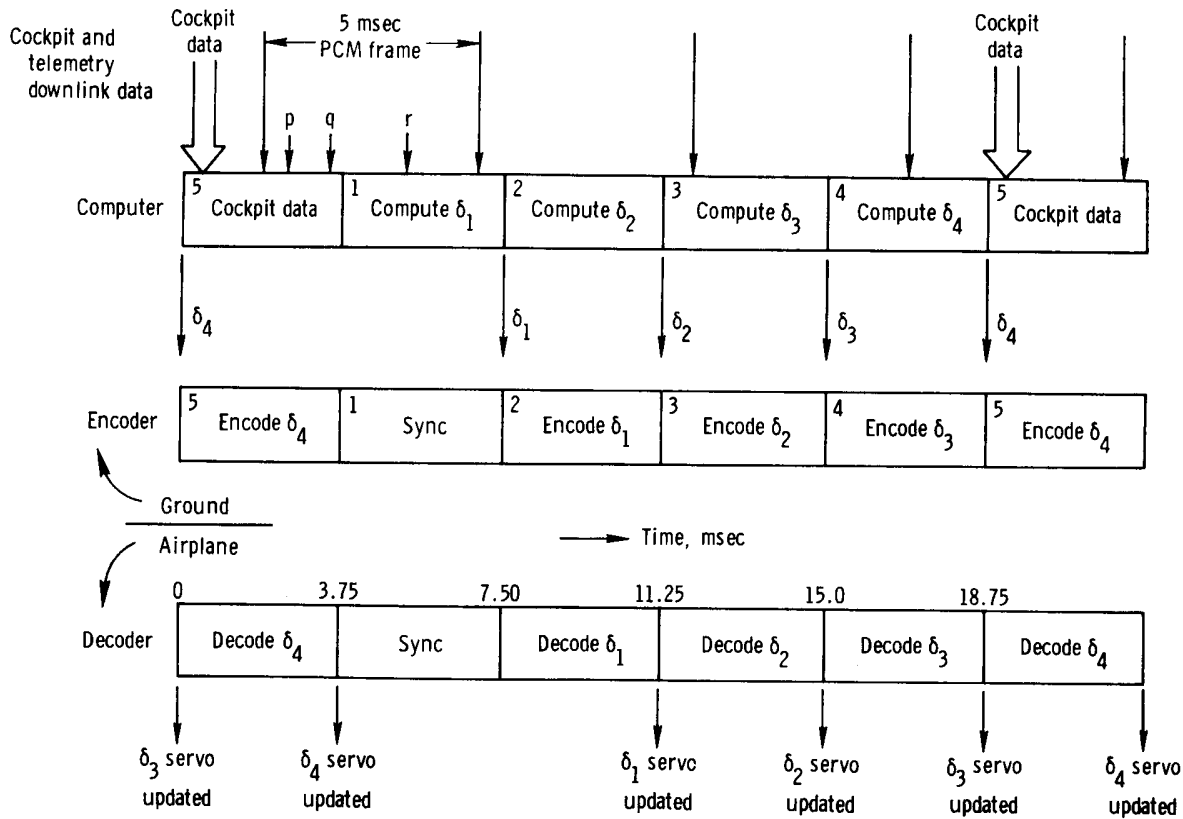

Figure 6. Computation sequence for RPRV system.

The throughput delay associated with the computer and encoder varies from 7.5 milliseconds to 12.5 milliseconds. The minimum delay occurs when a sensed variable enters the computer immediately before the beginning of the frame in which it would be used. The variable would be used to update the command signal during that 3.75-millisecond frame and would be transmitted to the test airplane to update the airplane's controls at the end of the following 3.75-millisecond frame. The maximum delay of 12.5 milliseconds occurs if the sensed variable is 5 milliseconds old before the current computation frame begins.

As an example of the approximate total lag through the system, from sensor output to control surface actuator command, the lag shown in the table on the next page would be accumulated for a 5-hertz signal with a vehicle located 75 kilometers from the ground station.

	Time delay, milliseconds
40-hertz analog prefilter	4.44
Downlink (PCM) encoding	.06
Transmittal to ground station	.25
Average computer/encoder throughput	10.00
Zero-order hold	9.40
Transmittal to airplane	.25
Average total delay	24.40

This time delay corresponds to a 44° phase lag at 5 hertz, an acceptable lag for most applications. If this lag is unacceptably large, some lead could be generated by programing a lead-lag filter in the digital computer.

All computations within a given frame, as well as background interrupt servicing (invisible to the FORTRAN program), must be performed within 3.75 milliseconds. If this time constraint is violated, the interrupt for that frame will occur before the FORTRAN program is ready to test for its occurrence. Then the FORTRAN program must wait for the next interrupt before it can begin the next computation frame. Thus the command in the following frame would not be updated.

SUBSCALE F-15 PROGRAM

The RPRV facility was used to flight test a 3/8-scale model of the F-15 airplane. The goal of the flight program was to investigate the model's high-angle-of-attack performance and its stalling and spinning characteristics. This program was an appropriate application of the RPRV technique to hazardous flight testing, in that it was possible to perform much of the model testing before spin flight tests were made on the full-scale F-15 airplane. The function of the RPRV ground computer in the subscale F-15 program was to simulate the full-scale F-15 flight control systems. The F-15 open-loop mechanical control system (MCS) and the closed-loop control augmentation system (CAS) modes, containing actuator dynamics, gearing schedules, gains, and shaping filters, were implemented by using the ground computer.

F-15 Model

A three-view drawing of the F-15 model is shown in figure 7. The model was built to be at least as stiff as the full-scale airplane to minimize structural resonance problems. Batteries powered all onboard systems, including the hydraulic actuators which positioned the control surfaces. The control surfaces consisted of left and right stabilators for pitch and roll control, ailerons for roll control, and twin rudders for yaw control. The control surface actuators had 10-hertz bandwidths. A detailed description of the model and instrumentation system is given in reference 3.
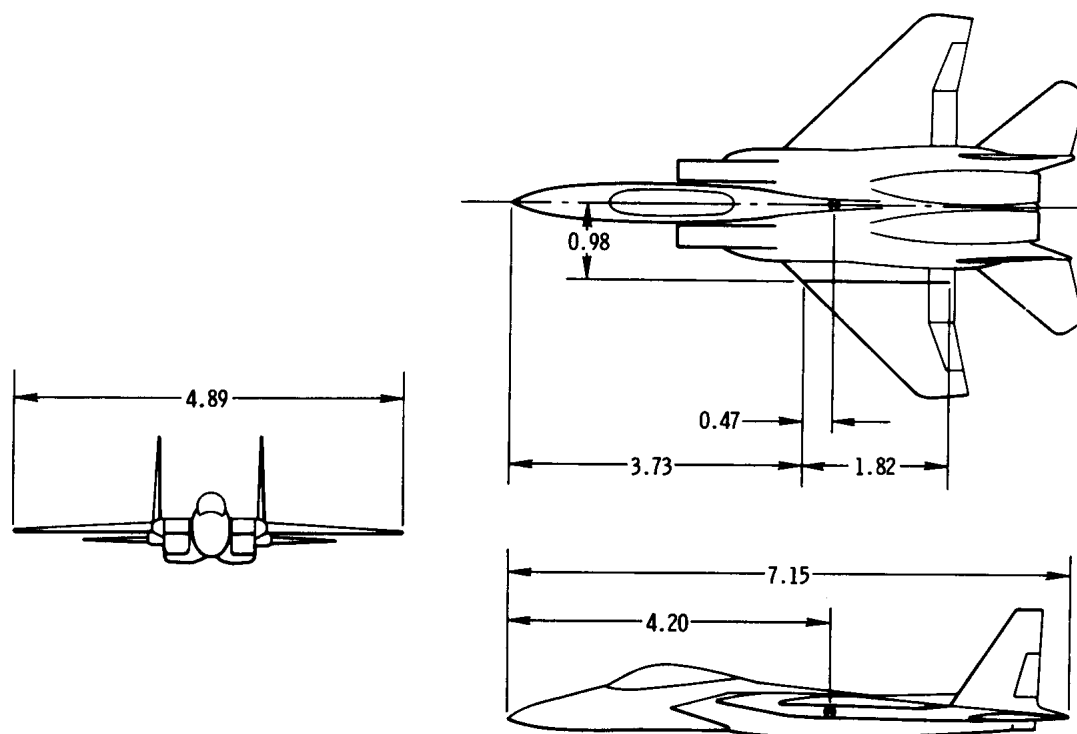
Figure 7. Three-view drawing of 3/8-scale-model F-15. Dimensions in meters.

Two center-of-gravity locations—at the 26-percent mean aerodynamic chord and at the 30-percent mean aerodynamic chord—were used. The 30-percent mean aerodynamic chord location is the most rearward center-of-gravity location in the full-scale F-15 airplane.

Weights and inertias were as close as practical to the values required for correct 3/8-scale inertial-force-to-gravitational-force scaling. Appendix A discusses this scaling technique and derives the corresponding scaling laws. The desired values of weight and inertia and the actual values for the two center-of-gravity locations are as follows:

	Desired value at 26-percent mean aero-dynamic chord	Actual value	
		26-percent mean aerodynamic chord	30-percent mean aerodynamic chord
Weight, N	7,668	10,964	10,951
I_X, kg-m^2	235	373	373
I_Y, kg-m^2	1,520	2,579	2,452
I_Z, kg-m^2	1,708	3,021	2,894
I_{XZ}, kg-m^2	-4.7	15.7	3.4

The differences between the actual and the desired values point up the difficulty of independently controlling the mass distribution of a flight vehicle while meeting all the proper geometrical and structural design load requirements. Strict adherence to the desired values was not necessary, since the ratio between model and full-scale atmospheric density is a factor in each of the mass and inertia scaling laws (table A2). Proper selection of model F-15 flight-test altitude could give a reasonable simulation of the full-scale F-15 at a different altitude.

To implement the full-scale F-15 CAS, the ground computer required three-axis rate signals, normal and lateral accelerations, and angle of attack from the model. Table 1 lists the input/output variables, and their ranges, required by the ground computer to implement the F-15 control system. The only analog prefiltering performed on board the model was with 40-hertz first-order low-pass filters on all signals. A simple wings-leveling autopilot was the only onboard control system. It was activated by loss of the carrier frequency of the uplink command signals.

Launch and Recovery Technique

The unpowered model was air-launched from a B-52 airplane at an altitude of 13,700 meters and had a flight time of approximately 5 minutes, depending on the number and types of maneuvers performed. The model was recovered with a midair parachute recovery system which was automatically deployed at 4600 meters altitude unless manual recovery was started earlier. The flight range of the model from the ground station was approximately 15 kilometers to 25 kilometers. During the launch sequence, the control surfaces of the model were locked in the launch configuration for 3 seconds. At the end of this interval, the uplink command signals became operative and the remote pilot took control of the model.

Simulation

A simulation of the RPRV system was required to check out RPRV programs and to provide pilot training and flight planning capability. The simulation was performed on the NASA Flight Research Center's central computer, utilizing its real-time simulation capability. The cockpit used in the simulation was designed to be as similar as possible to the RPRV facility cockpit. Six-degree-of-freedom equations of motion were mechanized, and the program was written to accept aerodynamic force and moment data in a general format. The airplane's continuous differential equations of motion were integrated numerically by the computer, using a second-order Runge-Kutta integration technique.

Two separate simulations of the RPRV system were implemented. The first, called the RPRV digital simulation, contained the basic aircraft simulation described above and a subroutine which simulated the control system modes of the RPRV computer program. The filters and actuator dynamics required for the basic modes and the F-15 control system modes were implemented in this subroutine by difference equations. The update rate of the difference equations was 53 samples per second. The processing of these equations simulated the operations performed by the RPRV computer.

TABLE 1.— INPUT/OUTPUT VARIABLES TO RPRV COMPUTER FOR 3/8-SCALE-MODEL F-15

Variable	Range
Cockpit inputs (10 bits)	
δ_{e_p}	-7.37 cm to 13.72 cm
δ_{a_p}	±10.16 cm
δ_{r_p}	±8.26 cm
F_{δ_e}	-111 N to 204 N
F_{δ_a}	±71 N
$\delta_{e_{trim}}$	-7.37 cm to 13.72 cm
$\delta_{a_{trim}}$	±10.16 cm
Telemetry downlink inputs (9 bits)	
α	-5° to 35°
p	±200 deg/sec
q	±100 deg/sec
r	±100 deg/sec
n_z	-3g to 6g
n_y	±1g
Telemetry uplink outputs (10 bits)	
δ_{a_c}	±20°
$\delta_{h_{L_c}}$	-27.5° to 15°
$\delta_{h_{R_c}}$	-27.5° to 15°
δ_{r_c}	±30°

16

The second simulation, called the analog CAS simulation, contained the basic aircraft simulation and a subroutine which simulated the operation of the F-15 analog CAS. The continuous differential equations which described the analog CAS were integrated, along with the airplane's equations of motion, at 200 samples per second. Both systems of equations were integrated by using the same second-order Runge-Kutta integration technique. The validity of the RAV system approach to flight testing was assessed by comparing the RPRV digital simulation of the F-15 CAS and the analog CAS simulation.

Since the subscale model flight program involved stalling and spinning, these maneuvers were simulated. Wind-tunnel aerodynamic data for angles of attack from 0° to 90° and angles of sideslip from -40° to 40° were used in the simulation, as well as a limited amount of wind-tunnel aerodynamic data for angles of attack from 0° to -90°. Thus stalls, departures, post-stall gyrations, and fully developed spins could be simulated to the extent of the validity of the aerodynamic data.

Because the RPRV computer program was coded in floating point FORTRAN, it was possible to incorporate the actual program into the RPRV digital simulation as a subroutine. Only minor modifications to the RPRV computer program were required to make it compatible with the flight planning simulation.

The central computer's UPDATE feature was another aid in modifying the RPRV program. An UPDATE file of the entire simulation program was created, including a representation of the actual RPRV program card deck as a subroutine. The UPDATE feature permitted individual cards to be inserted or deleted from the UPDATE file and the resulting file to be compiled by the FORTRAN compiler. This enabled modifications to be made in the RPRV program in less than 5 minutes. When a final configuration was attained for an RPRV flight, a hard-copy record of the individual changes to the original RPRV card deck was available. This method of operation, coupled with the debugging capability of the RPRV computer's FORTRAN compiler, provided a high level of confidence in the modified RPRV program software.

USE OF REMOTELY AUGMENTED VEHICLE SYSTEM WITH THE SCALE-MODEL F-15

The RAV system can be used to control remote vehicles in a closed-loop, high-bandwidth mode using telemetry downlink and uplink data. This capability gives the RPRV facility an added dimension over an open-loop uplink control mode but requires that attention be given to the stability of the system. This section discusses the use of the RPRV facility in this remote augmentation mode.

Digital Filtering Technique

Simulation of analog components of a flight control system on a digital computer requires the use of a technique of discrete representation of continuous transfer functions. The technique used in the RPRV/RAV system was to transform continuous transfer functions, $G(s)$, into discrete transfer functions, $G(z)$, which were then implemented in the control computer as difference equations. The digital filtering algorithm used to simulate the scale-model F-15 analog control system is described

in appendix B. The algorithm is an extension of the technique referred to in reference 4 as "bilinear transformation with frequency prewarping" and in reference 5 as the matched z-transform. The algorithm implements an exact conformal mapping from the s-plane to the w-plane, followed by the bilinear transformation:

$$w = \frac{z - 1}{z + 1}$$

The exact mapping of the s-plane to the w-plane yielded digital filters with magnitude and phase characteristics which were good approximations of the original continuous transfer functions. The resulting digital filters were similar to those which would be obtained by using the Tustin method, an alternative filtering algorithm (ref. 5), but were superior in several respects, as noted in appendix B.

The filtering algorithm described was also used to implement required digital compensation, aside from any requirement for simulating an analog function. In this application, frequency domain requirements such as notch filters may be translated directly to a digital filter by the algorithm. For example, digital notch and low-pass filters were required for the closed-loop rate damper and CAS modes. The z-plane transfer functions of the digital filters were derived by the filtering algorithm. These transfer functions contained the coefficients required for mechanizing the filters by means of difference equations in the RPRV program control laws. The general form of the notch filter was

$$G(z) = \frac{K''(z^2 - 2 \cos bT\, z + 1)}{z^2 - 2e^{-cT} \cos dT\, z + e^{-2cT}}$$

where

$$K'' = \frac{1 - 2e^{-cT} \cos dT + e^{-2cT}}{2 - 2 \cos bT}$$

in which b specifies the notch frequency and location of the positive complex zero on the s-plane imaginary axis, and c and d specify the s-plane coordinates of the desired poles. The general form of the low-pass filter was

$$G(z) = \tfrac{1}{2}\left(1 - e^{-\beta T}\right)\frac{(z + 1)}{\left(z - e^{-\beta T}\right)}$$

where β specifies the s-plane coordinate of the desired real pole.

Remote Augmentation Modes for the Scale-Model F-15

Several tasks were required of the RPRV ground computer in the scale-model F-15 program. It was necessary to have two basic control modes available that were specifically designed for the research function of the scale model and not related to the full-scale airplane's control system. The MCS and CAS modes were not well

18

suited to stability and control maneuvers because of gearing schedules and inter-connects which modified and restricted control surface authority as a function of flight condition, particularly at high angles of attack. The computer was also required to simulate the full-scale airplane's open-loop MCS and closed-loop CAS for the stall and spin testing. Motion of the control surfaces can have a marked influence on an airplane's propensity to experience a spin departure. The basic control modes and the F-15 control system modes were implemented in the computer program as four different control modes and placed under the remote pilot's control by means of the mode control panel.

Basic modes.— As shown in figure 8, the two upper rows of selector buttons on the mode control panel are the basic modes, and the two lower rows are the F-15 control system modes. The basic modes were required to provide (1) a simple control system for the initial checkout of the RPRV systems and (2) the full control authority of the airplane throughout the model's flight envelope to obtain stability and control data. The open-loop airplane is lightly damped in both the longitudinal and lateral-directional axes at high angles of attack, so the requirement to obtain useful stability and control data necessitated high damper gains. These gains were implemented in the rate damper mode. Stability and control maneuvers were performed by using the damper system to establish a trimmed flight condition and switching the damper gain in one or more axes to a low value or zero before the maneuver was started.

Block diagrams of the basic modes for the pitch axis are shown in figure 9(a) and for the roll and yaw axes in figure 9(b). The pilot's longitudinal stick displacement is modified by a nonlinear gearing schedule which commands the stabilators collectively. The nonlinear gearing schedule, shown in figure 10, was implemented to provide good model handling qualities in the launch condition ($\delta_h \approx 0°$) and full stabilator authority of 15° to -27.5° in the computer direct and rate damper modes. These are the maximum positive and negative stabilator deflections that can be commanded by the full-scale airplane's control system. Full stabilator authority was provided because it was intended to obtain stability and control data in these modes at the maximum angle of attack early in the flight program. The gearing schedule was mechanized in the RPRV computer as the sum of linear and quartic factors of δ_{e_p}.
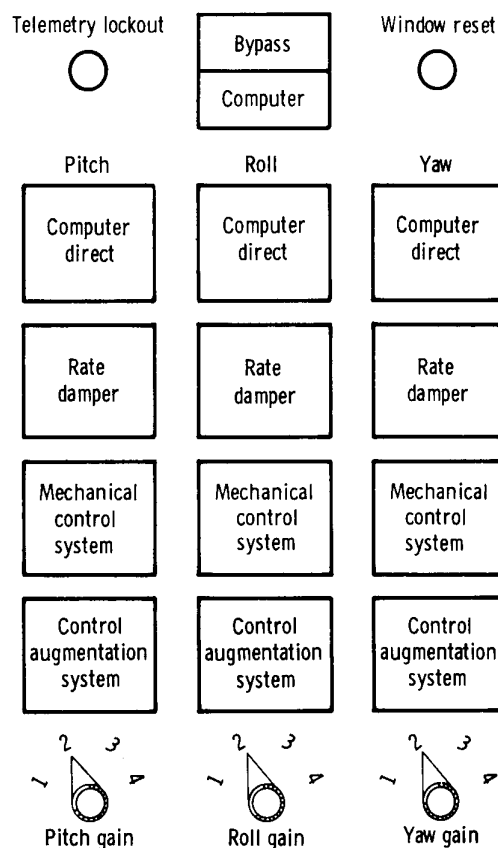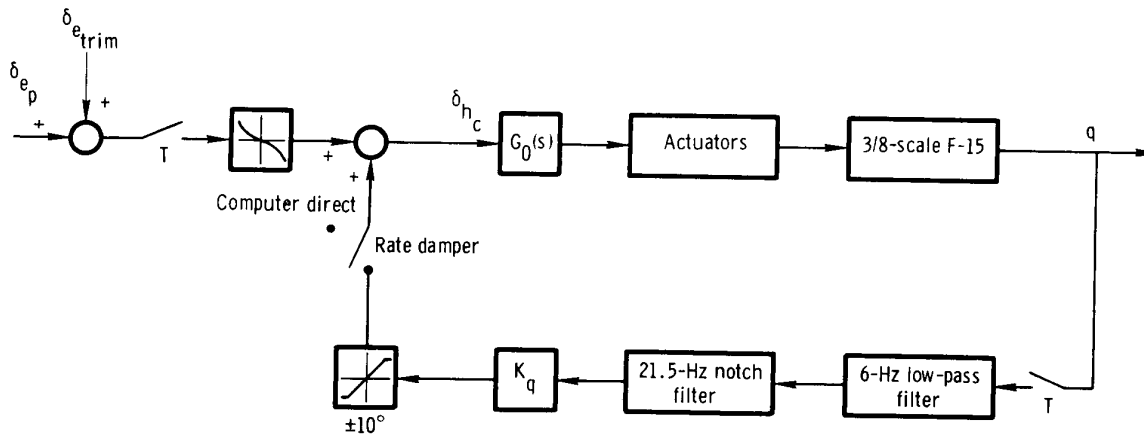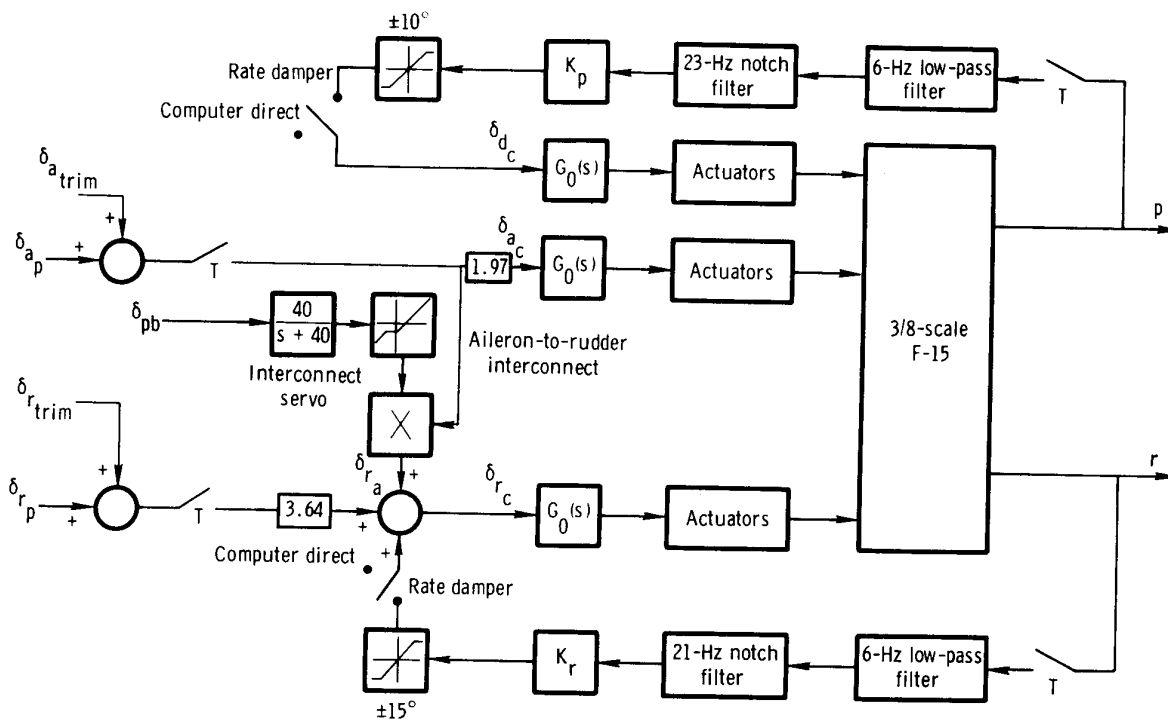
Figure 8. Mode control panel.

19

(a) Pitch axis.

(b) Roll and yaw axes.

Figure 9. Block diagrams of the computer direct and rate damper modes.

20

Forward stick
limit

15

10

5

-8   -4   0   4   8   12   16

δ_{e_p}, cm

-5

δ_h, deg

-10

-15

-20
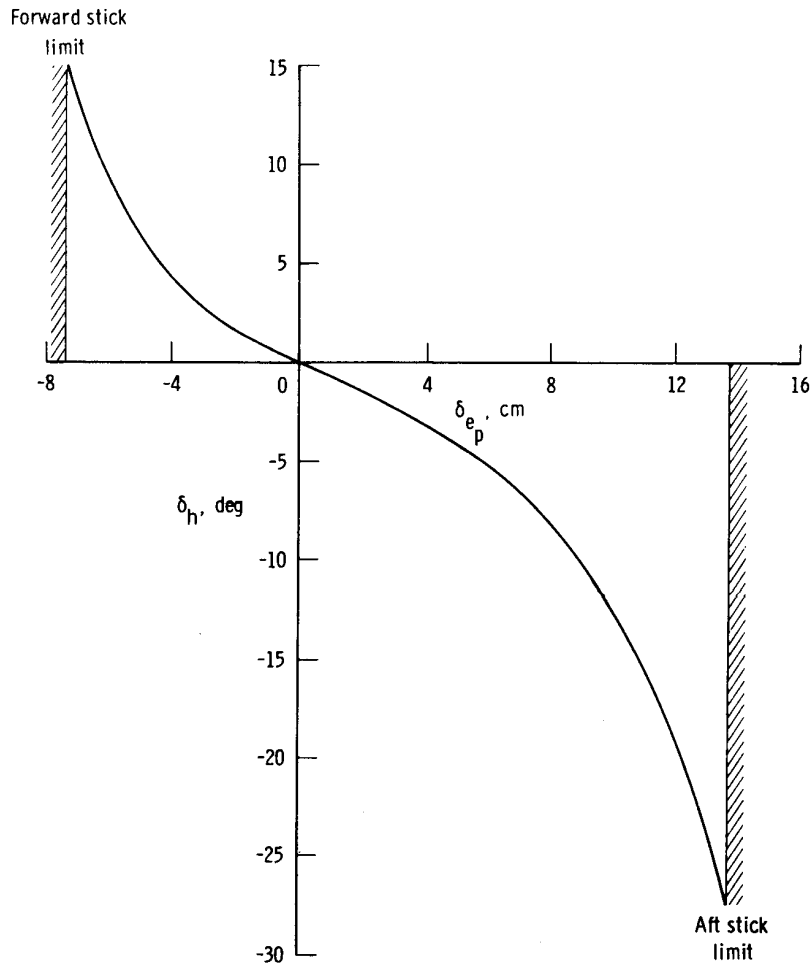
-25

Aft stick
limit

-30

Figure 10. Nonlinear longitudinal stick-to-stabilator gearing for the computer direct and rate damper modes.

The pilot's lateral stick displacement, δ_{a_p}, commanded the ailerons and the rudders through an aileron-to-rudder interconnect. Since the F-15 MCS mode contained an interconnect schedule, the basic modes used this interconnect by executing the same code as used by the MCS mode for this function. The interconnect gain was scheduled as a function of pitch boost servo output, δ_{pb}, a parameter generated in the MCS code approximately proportional to the pilot's longitudinal stick position. The pilot's rudder pedals also controlled the rudders.

In the rate damper mode mechanization (fig. 9) damper commands were summed with the computer direct mode pilot commands. The rate damper mode implemented angular rate feedback in which pitch rate, q, was fed to the collective stabilators, roll rate, p, was fed to the differential stabilators, and yaw rate, r, was fed to the rudders. Each of the rate gyro signals was low-pass-filtered at 6 hertz and notch-filtered to eliminate the dominant structural resonance near 20 hertz. Amplitude

authority limits of $\pm 10°$, $\pm 10°$, and $\pm 15°$ were implemented in the pitch, roll, and yaw axes, respectively. Maximum rate damper gains used are listed in table 2 together with the gains implemented in the CAS mode, which will be discussed later. All the functions of the computer direct and rate damper modes shown in figure 9 were programed in the RPRV computer.

TABLE 2.— MAXIMUM RATE DAMPER GAINS AND
SCALE-MODEL F-15 CAS GAINS

Quantity	Maximum rate damper gain	Scale-model F-15 CAS gain
K_q, sec	0.4	0.133
K_p, sec	-0.8	-0.077
K_r, sec	4.0	- - -
K_{r_s}, sec	- -	0.613
K_{C*}, deg/g	- -	1.0
K_{n_y}, deg/g	- -	9.2

Scale-model F-15 modes.— Simulation of the full-scale F-15 control system required scaling of the system gains and characteristic frequencies in order to maintain the proper ratios of inertial to gravitational force. Appendix A derives scaling laws for the augmentation feedback control gains and shows that only angular rate feedback gains need modification. For example, the correct scaling for pitch rate feedback gain is

$$K_q = a^{\frac{1}{2}} K_{q_f}$$

where a is the model scale factor and K_{q_f} is the pitch rate feedback gain for the full-scale F-15 airplane. The decrease in gain reflects the increased angular rates experienced by the model. Also, all the critical frequencies of the full-scale airplane's flight control system dynamic components (actuators and filters) must be increased by $a^{-\frac{1}{2}}$ to reflect the time scaling of the model. Block diagrams of the F-15 MCS and CAS modes are shown in figures 11(a) and 11(b) for the pitch and the roll and yaw axes, respectively. The figures show the system implemented in the RPRV computer and include the critical frequency and rate feedback scaling.

The analog transfer functions of the servo actuators and shaping filters are also shown in figure 11 and are summarized in table 3. The transfer functions were simulated by difference equations which were implemented by using the digital filtering algorithm described in appendix B. The position limits and rate limits of the actuators were also simulated and are listed in table 3.

22
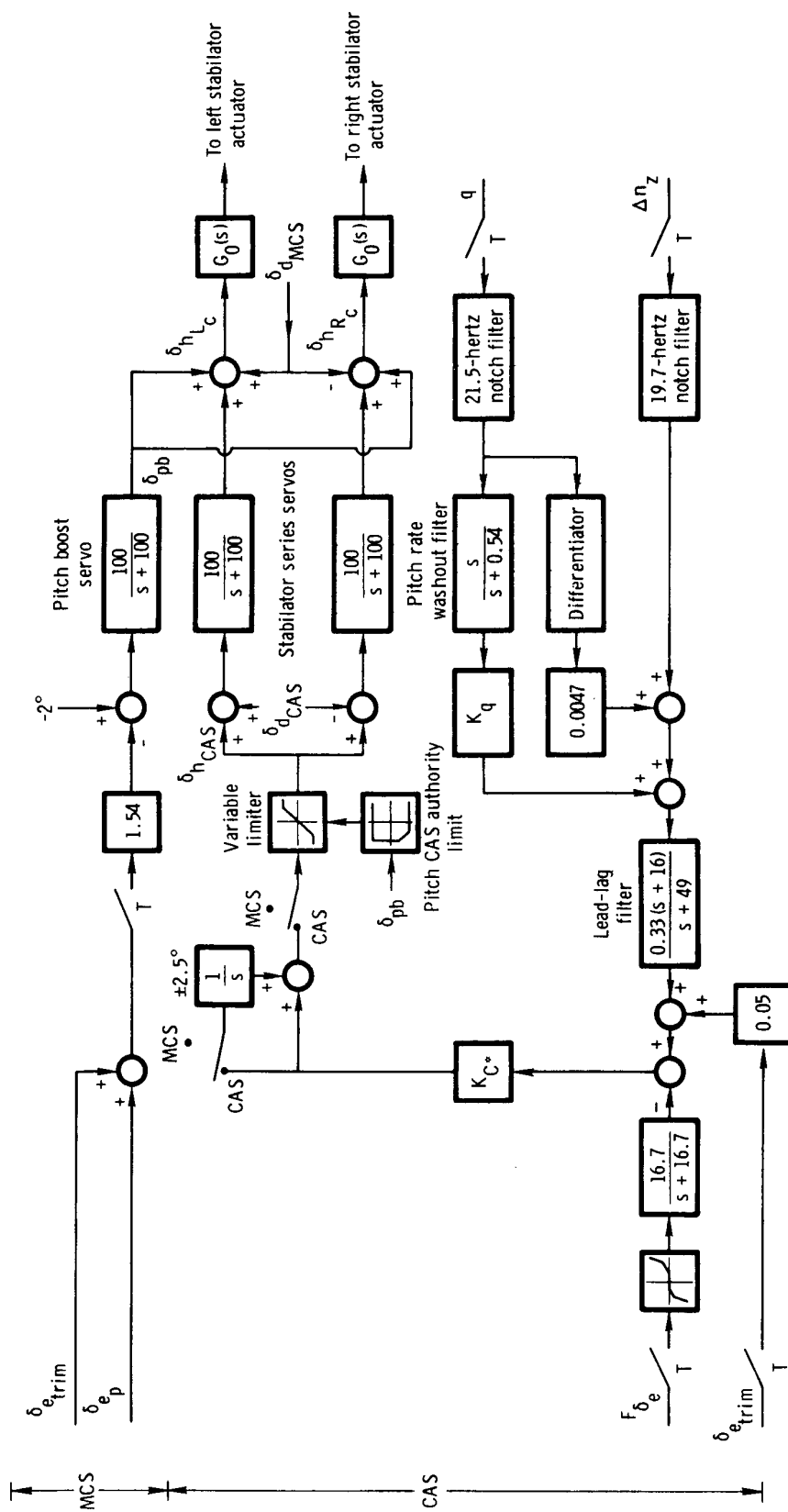
Figure 11. Block diagram of the scale-model F-15 control system.

(a) Pitch axis.

23

(b) Roll and yaw axes.

Figure 11. Concluded.

TABLE 3.— CHARACTERISTICS OF THE SERVOS AND SHAPING FILTERS
FOR THE SCALED F-15 FLIGHT CONTROL SYSTEM

Servos and shaping filters	Transfer function	Position limit, deg	Rate limit, deg/sec
Pitch boost servo	$\dfrac{100}{s + 100}$	15, -25	±320
Roll boost servo (single surface)	$\dfrac{100}{s + 100}$	±20	±320
Stabilator series servos	$\dfrac{100}{s + 100}$	±10	±57
Rudder series servo	$\dfrac{100}{s + 100}$	±15	±146
Interconnect servo	$\dfrac{40}{s + 40}$	- - -	±57
Lead-lag filter	$\dfrac{0.33(s + 16)}{s + 49}$	- - -	- - -
Pitch rate washout filter	$\dfrac{s}{s + 0.54}$	- - -	- - -
Yaw rate washout filter	$\dfrac{s^2}{(s + 0.54)^2}$	- - -	- - -
Differentiator	$\dfrac{s}{1 + 2\dfrac{0.3s}{37} + \dfrac{s^2}{37^2}}$	- - -	- - -

Mechanical control system: The MCS mode was a simulation of the primary flight control system of the full-scale F-15 airplane in which the pilot was assisted in pitch and roll control by hydraulic power boost servos. These boost servos were simulated on the ground computer for the scale-model MCS mode. The pitch boost servo output, δ_{pb}, was combined with the roll MCS command, $\delta_{d_{MCS}}$, to form the commands to the left and right stabilizer power actuators, $\delta_{h_{L_c}}$ and $\delta_{h_{R_c}}$. These power actuators were duplicated on board the scale-model F-15 by the model's hydraulic actuators and were not simulated in the ground computer. Similar functions were performed by the aileron and rudder actuators.

The longitudinal stick position controlled the collective stabilators, and the lateral stick position controlled the ailerons and differential stabilators. The rudders were controlled by the rudder pedals and the aileron-to-rudder interconnect. Lateral control authority was scheduled as a function of the lagged pitch boost servo output, δ'_{pb}, and resulted in the authority being restricted at aft and forward longitudinal stick positions (fig. 12). The interconnect was also scheduled as

a function of δ'_{pb} (fig. 13) and resulted in rudder commands proportional to lateral stick deflection.
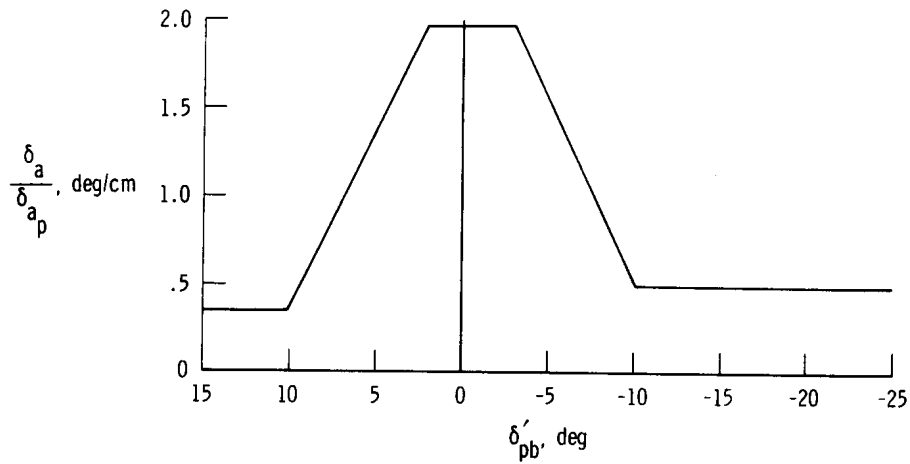

Figure 12. MCS lateral control gearing schedule as a function of lagged pitch boost servo output.
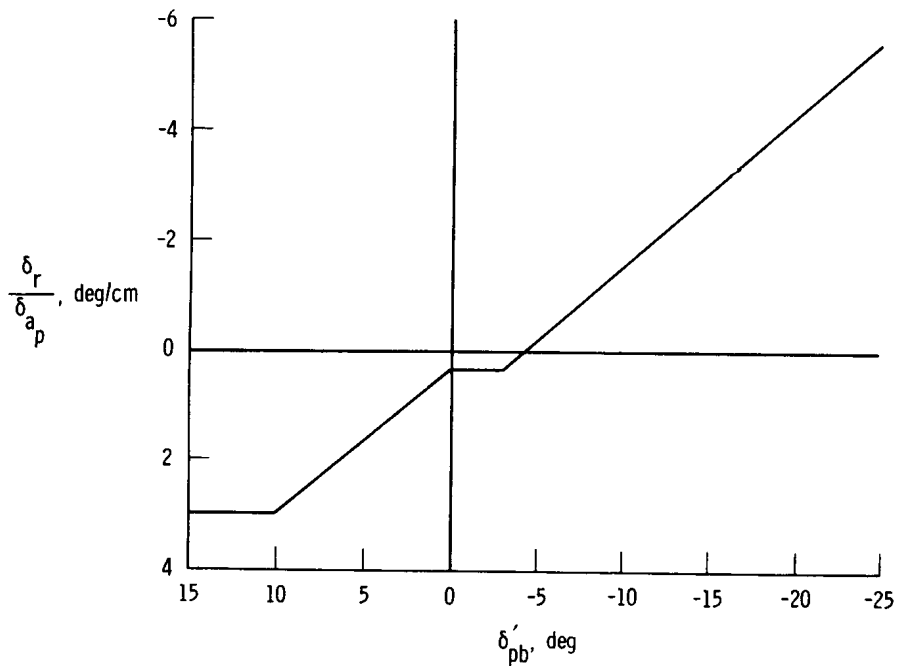

Figure 13. MCS aileron-to-rudder interconnect gearing as a function of lagged pitch boost servo output.

Control augmentation system: The CAS utilized pitch, roll, and yaw rates and normal and lateral accelerations as feedback variables. Each of these five signals was notch filtered to suppress the approximately 20-hertz resonance. The three rate gyro signals used the same notch filters as those for the rate damper mode (described previously).

The pitch CAS command was composed of a modified form of the blended normal acceleration and pitch rate response parameter, commonly referred to as C^* (ref. 6), and commanded normal acceleration derived from longitudinal stick force, F_{δ_e}. The commanded normal acceleration signal was derived by passing the longitudinal stick force, F_{δ_e}, through a dual-gradient gearing schedule and a first-order shaping filter.

A stall inhibiter function is also included in the full-scale F-15 CAS to provide nose-down stabilator deflection when angle of attack or washed out pitch rate, or both, exceed a preset level. For the flight tests described in this report, this stall inhibiter function was disabled in the RPRV computer program because the intent of the program was to investigate the stalling and spinning characteristics of the model. The pitch CAS command was passed through a proportional plus integral feed-forward network and limited by the schedule shown in figure 14 to form the pitch CAS command, $\delta_{h_{CAS}}$, which was summed with the roll CAS command, $\delta_{d_{CAS}}$. The combined pitch and roll CAS commands positioned the series servos. The outputs of the servos were then summed with the pitch boost servo output and the MCS differential stabilator signal to form the left and right stabilator commands, $\delta_{h_{L_c}}$ and $\delta_{h_{R_c}}$, which were the uplink commands required for the RPRV system operation.
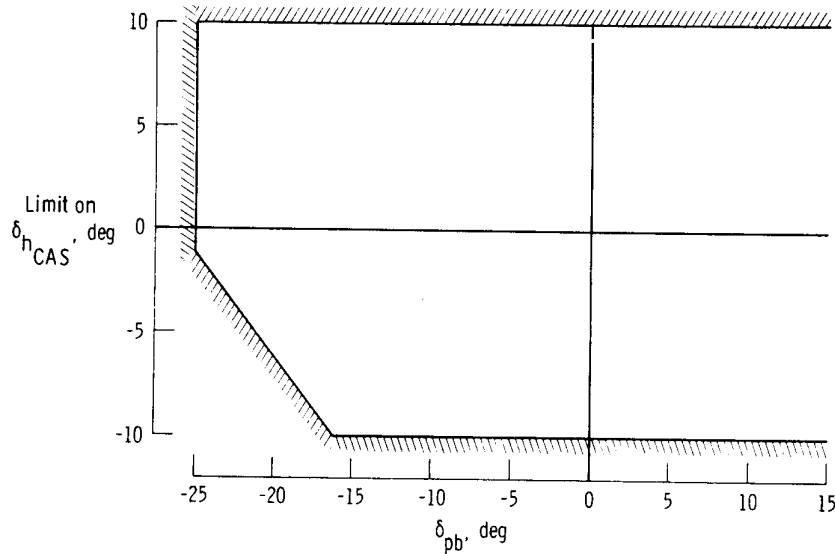

Figure 14. Pitch CAS authority limit as a function of pitch boost servo output.

The roll CAS command to the differential stabilator was formed by comparing roll rate to commanded roll rate from the lateral stick force. The commanded roll rate signal was derived by passing lateral stick force, F_{δ_a}, through a dual-gradient gearing schedule. The resulting roll rate error signal was limited by the roll CAS angle-of-attack schedule shown in figure 15 to form $\delta_{d_{CAS}}$ and summed with the pitch CAS command, $\delta_{h_{CAS}}$.
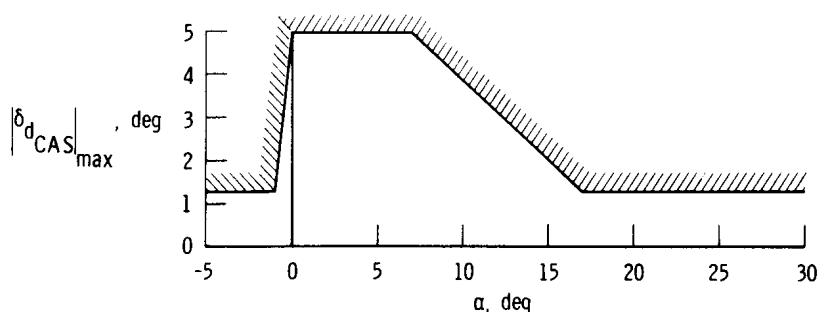

Figure 15. Roll CAS authority limit as a function of angle of attack.

In the yaw axis CAS mode, rudder pedal gearing was effectively doubled over that of the MCS mode. Lateral acceleration and washed out stability axis yaw rate were fed to the rudders. The stability axis yaw rate signal was computed as $r_s = r - \alpha p$.

To account for different accelerometer locations in the full-scale and scale-model F-15 vehicles, pitch rate and yaw rate were differentiated and summed with n_z and n_y, respectively, to simulate lever arm effects.

The full-scale CAS contained an automatic "downmoding" from CAS to MCS for spin departure prevention which was activated when the yaw rate exceeded ±42 deg/sec. For the scale-model F-15 the scaled yaw rate was ±70 deg/sec. The effect of the downmoding was to restrict control authority and deactivate feedback controls, since full control authority or feedback augmentation, or both, could enhance the departure rather than oppose it. This function was easily programed into the RPRV system.

Software Mechanization

The scale-model F-15 computer program occupied 100 percent of the available core of the RPRV program and had a duty cycle of approximately 90 percent of the available computation time. The allocation of the RPRV computer's 16K memory for the subscale F-15 flight program is shown in figure 16. Note that the FORTRAN main program was the largest single unit in the computer, requiring 6500 words.

The core required by the resident opera-
ting system and the loader could not be
utilized during real-time RPRV operation
and may be viewed as the cost of the
FORTRAN programing capability. This
was not really a disadvantage because
the general purpose minicomputer mem-
ory could have been expanded if a larger
flight program were required. All con-
stants, digital filter coefficients, and com-
binations of constants required for the
RPRV program were precomputed in a
separate FORTRAN data program on the
RPRV computer and processed in an off-
line batch processing mode.

Words

1,900	Resident operating system
800	Common
1,700	Loader
3,700	Run-time mathematics and utility routines
1,400	Assembly subroutines
6,500	FORTRAN main program
300	Pointers

Total   16,300

Figure 16. RPRV computer memory map for scale-model F-15 program.

Wherever possible, the computations
performed by the RPRV program were in
engineering units using floating point
arithmetic. This eliminated the require-
ment of variable scaling and problems with arithmetic overflow. The relatively slow
floating point execution time (approximately 75 microseconds) of the RPRV computer
did not permit the entire RPRV program to be coded in floating point, so several
functions, including the digital notch filters, were coded in scaled fixed point
FORTRAN.

Analysis and Design

Two primary objectives of the scale-model F-15 flight program were to obtain
stability and control data for the full-scale airplane and to simulate the operation of
the F-15 flight control system in the high-angle-of-attack stall-spin region. Both
of these objectives required the use of the remote augmentation capability of the
RPRV system. As noted previously, to obtain high-quality stability and control data
at these high angles of attack, it was necessary to implement a relatively high gain
rate damper mode to stabilize the vehicle before the maneuvers were started. Also,
the CAS mode had significant effects on the high-angle-of-attack response of the
vehicle. Thus it was necessary to make a limited analysis of both augmented modes
to insure proper operation of the systems. The analysis discussed in this section is
for the 26-percent mean aerodynamic chord center-of-gravity location on the model.

Figure 17 is a z-plane plot of the location of the response modes of the open-loop
airplane as a function of trimmed angle of attack. The short-period, Dutch roll, phu-
goid, roll, and spiral modes are shown. The approximate s-plane coordinates are
included for reference. The stability boundary is indicated by the portion of the unit
circle. The open-loop natural frequencies of the airplane decrease with increasing
angle of attack from $\alpha \approx 3°$ to $\alpha \approx 17°$. Above $\alpha \approx 17°$ the short-period and Dutch roll
modes remain very lightly damped with a frequency of approximately 2 radians per
second over a large range of angle of attack, whereas the roll and spiral modes

continue toward a lateral phugoid mode. Minimum stability for the short-period mode is at α ≈ 26° and for the Dutch roll mode at α ≈ 28°. The phugoid mode is only slightly affected by angle of attack. Obviously, the lightly damped oscillatory modes would respond to pilot inputs or aerodynamic buffet, so a damper system was required to augment the damping of the vehicle.
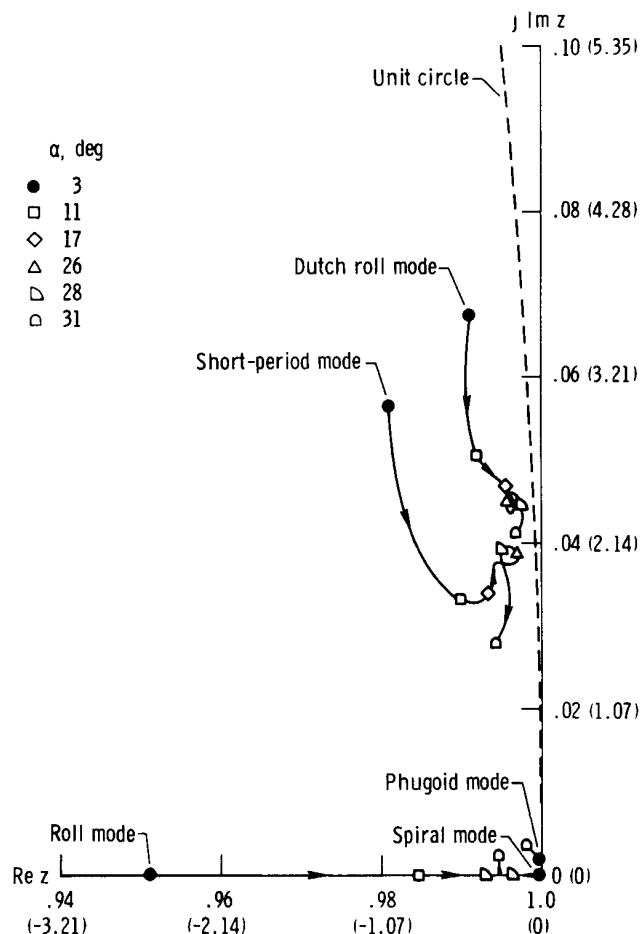

Figure 17. Root locus (z-plane) of response modes of scale-model F-15 as a function of trimmed angle of attack. (Approximate s-plane coordinates given in parentheses.)

Rate damper system. — The short-period mode was easily damped by using a pitch rate feedback to the stabilators. Figure 18 shows the z-plane root locus of this feedback for α = 3° and α = 26°. The actuator dynamics and filters shown in figure 9(a) were included. A maximum gain of 0.4 second was chosen. The pilot was able to select lower gains by using the pitch gain switch on the mode control panel.

Damping the Dutch roll mode proved to be difficult because the yaw rate damper was ineffective at angles of attack above 15°. Figure 19 shows the z-plane root locus of yaw rate feedback to the rudders for α = 3° and α = 28°. The actuator dynamics

and filters shown in figure 9(b) were included. The complex zero of the $\frac{r}{\delta_r}(z)$
transfer function effectively cancels the Dutch roll pole at high angles of attack. In addition, the rudder control power drops rapidly at these angles of attack.
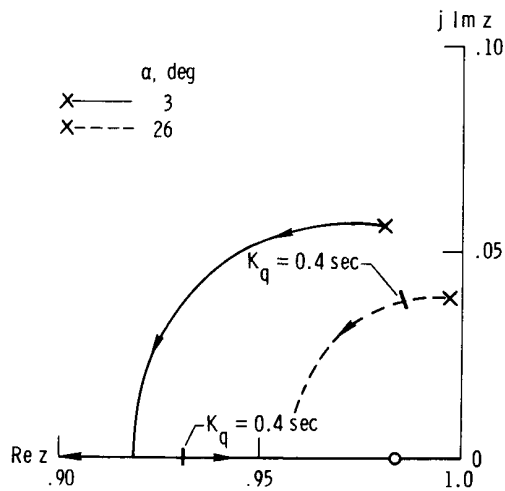

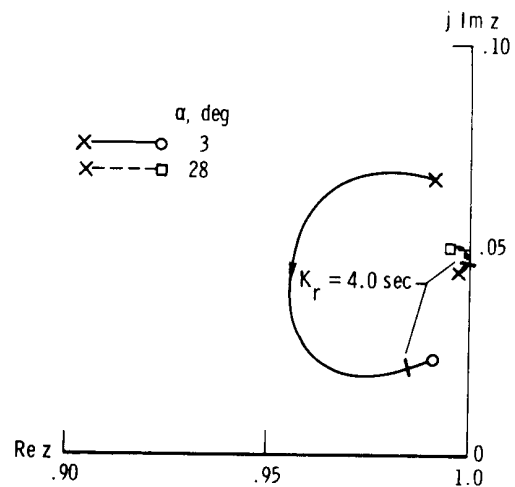Figure 18. Root locus (z-plane) of pitch rate damper short-period mode for α = 3° and 26°.

Figure 19. Root locus (z-plane) of yaw rate damper Dutch roll mode for α = 3° and 28°.

Although the yaw damper proved ineffective in damping the Dutch roll mode at high angles of attack, the roll damper was very effective. Figure 20 shows the z-plane root locus of roll rate feedback to the stabilators for α = 3° and α = 28°. Actuator dynamics and filters were included. Although the roll damper has little effect on the Dutch roll pole below α ≈ 15°, it is very effective at higher angles of attack. A maximum gain of 0.8 second was selected, which is considerably higher than the scaled roll CAS gain of -0.077 second.

Although the high roll damper gain stabilized the Dutch roll mode, it aggravated the coupled roll-spiral mode (lateral phugoid) at α ≈ 30° and caused a low-frequency heading stability problem. The yaw damper was beneficial
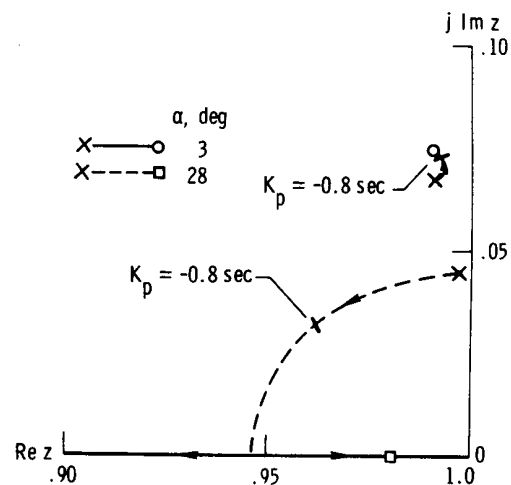

Figure 20. Root locus (z-plane) of roll rate damper Dutch roll mode for α = 3° and 28°.

in damping this lateral phugoid, as shown in figure 21. The figure shows the z-plane root locus of the lateral phugoid at $\alpha = 28°$ due to roll rate feedback to the stabilators, followed by the root locus of yaw rate feedback to the rudder. The maximum yaw rate gain of 4.0 seconds was selected to position the lateral phugoid roots.
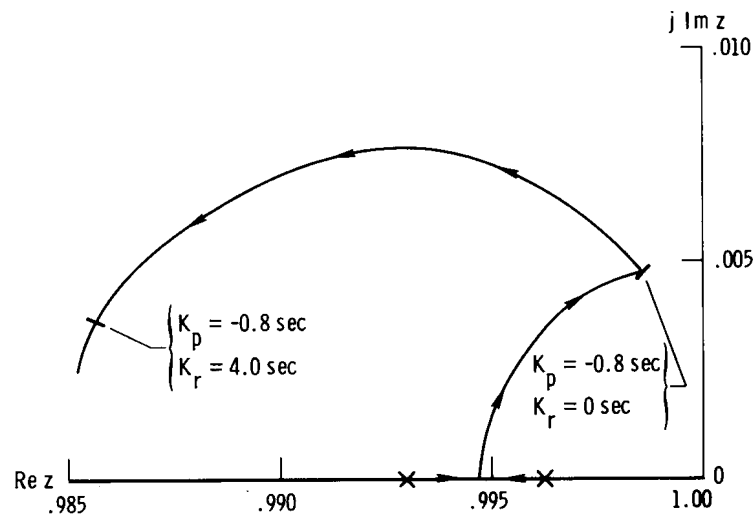

Figure 21. Root locus (z-plane) of lateral phugoid mode for roll rate feedback to stabilators followed by yaw rate feedback to rudder at $\alpha = 28°$.

The high maximum roll and yaw gains chosen for the rate damper mode reflected the relative uncertainty concerning the model's lateral-directional aerodynamics when trimmed at full aft longitudinal stick. The pilot was able to select lower roll and yaw damper gains through the gain switches on the mode control panel.

Control augmentation system. — The CAS mode introduced feedback variables into the remote augmentation system in addition to those required for the rate damper mode. Normal and lateral acceleration feedbacks and angle-of-attack scheduling of roll rate feedback were required, as shown in figure 11. The effectiveness of the rate feedbacks in the CAS mode in damping vehicle motions was similar to that for the rate damper mode. The crossfeed of roll rate to the rudder in the stability axis yaw rate feedback was a key difference between the rate damper mode and the CAS mode, aside from the higher gains used in the rate damper mode. The z-plane root locus of the Dutch roll mode for the stability axis yaw rate feedback to δ_r is shown in figure 22 for $\alpha = 3°$ and $28°$. The filters and actuator dynamics shown in figure 11 were included, and the yaw CAS gain ($K_{r_s} = 0.613$ sec) is indicated on the locus. The damping of the Dutch roll mode is increased at both angles of attack by the stability axis yaw rate feedback.

In addition to the rate feedbacks, the CAS uses normal and lateral acceleration feedbacks to provide good handling qualities. No difficulty was foreseen in using these signals for rigid body control; however, the use of acceleration feedbacks may

have caused structural resonance problems. (The implementation of notch filters to suppress structural resonance was described previously.)
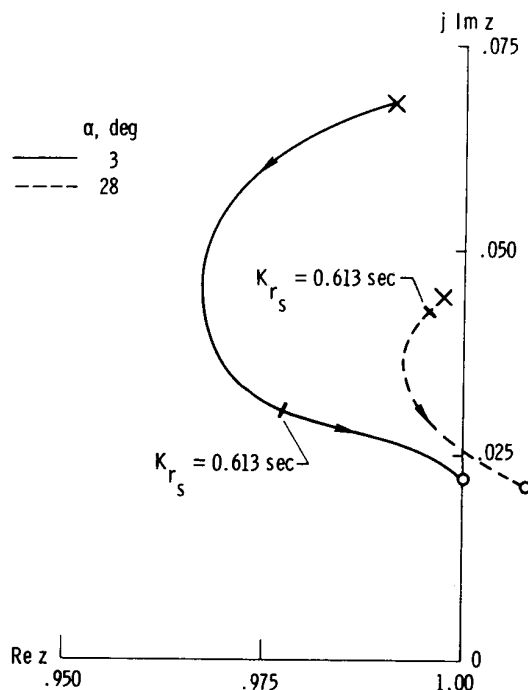

Figure 22. Root locus (z-plane) of stability axis yaw rate feedback to rudder for α = 3° and 28°.

A primary objective of the scale-model F-15 program was to achieve a valid simulation of the F-15 analog flight control systems. No attempt was made to investigate modifications to the CAS mode. The ability of the remote augmentation system to simulate the analog CAS of the full-scale F-15 airplane is indicated in figure 23, which compares step responses of the pitch CAS for the RPRV digital simulation and the analog CAS simulation. No attempt was made to adjust the gains or constants of the RPRV digital simulation to achieve a better "match" with the analog CAS simulation.

Ground Testing and Checkout

Before flight the RPRV program software was extensively checked and tested to insure that computation time was not excessive and that the gearing schedules and gain schedules operated correctly.

To identify resonance problems, a ground vibration test was made on the vehicle. Symmetric vibration modes were mapped with frequencies of 15.4 hertz, 16.2 hertz, 18.2 hertz, 21.0 hertz, 39.0 hertz, and 51.0 hertz. The 21.0-hertz mode had a noticeable horizontal-stabilator motion which was sensed by the pitch rate gyro and normal accelerometer. The 18.2-hertz mode was also prominent. The strong
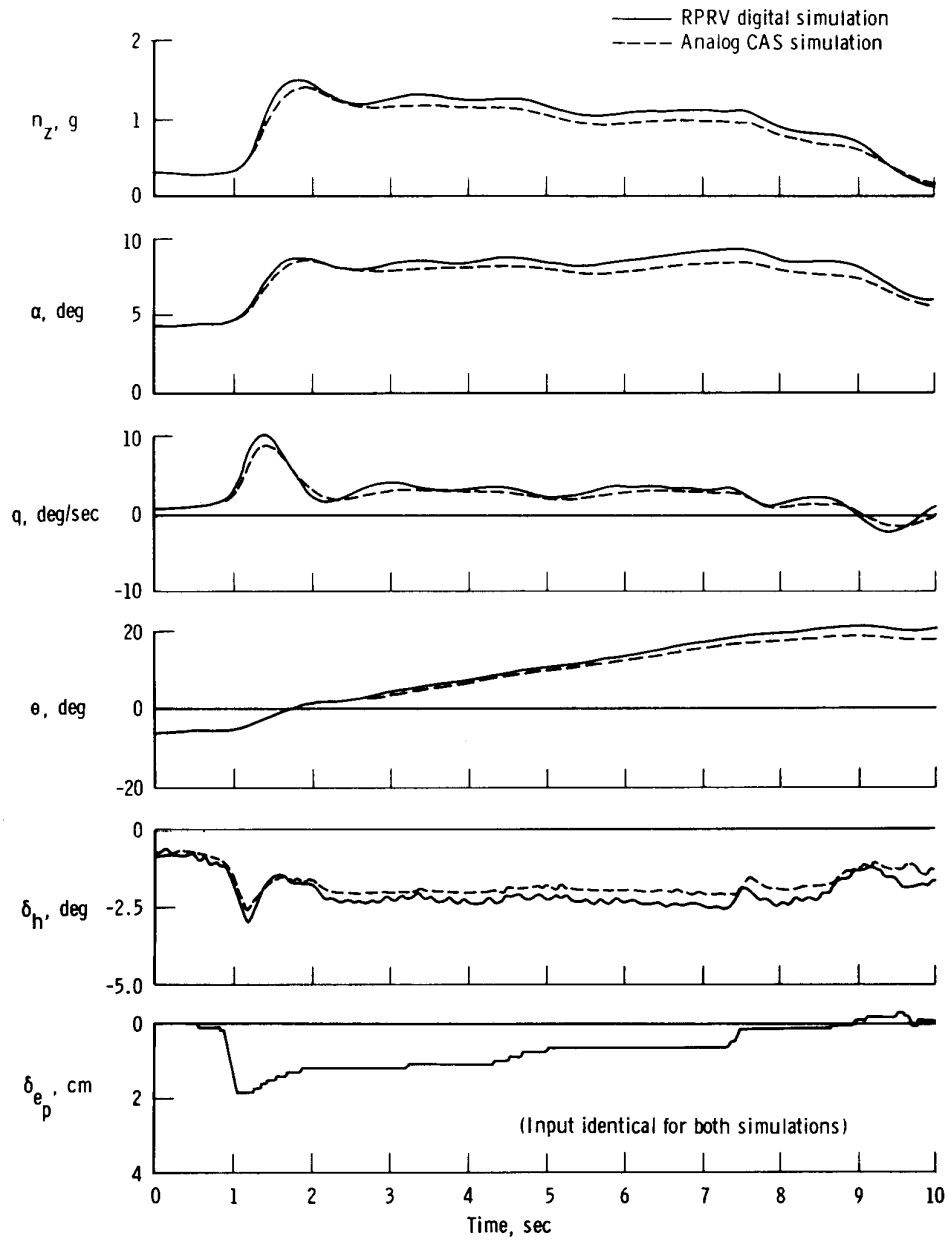
Figure 23. Comparison of scale-model F-15 pitch CAS response to pilot input for RPRV digital simulation and analog CAS simulation.

coupling between stabilator motion and sensor pickup of the modes near 20 hertz indicated a possible problem in the augmented modes.

Before the flights in which the rate damper and CAS modes were used, structural resonance tests were made on the closed-loop system to determine stability margins. The test feedback gains were several times larger than those to be used in flight. The RPRV flight program was coded to branch around the notch and low-pass filters in the feedback loops if a sense switch was set. Thus the effect of the filters on the system stability could be assessed. The only structural resonance observed in the tests was a symmetrical mode which was driven unstable by pitch rate feedback to the stabilators at a frequency of approximately 20 hertz. For the pitch rate damper mode with no notch or low-pass filtering, the instability occurred at a gain of 1.0 second. When the notch filter was added, the 20-hertz instability was no longer seen, but a 10-hertz neutrally damped oscillation occurred at a slightly higher gain. No structural mode had been identified at this frequency, and the oscillation was traced to a mass unbalance of the stabilators which caused a "tail-wags-dog" oscillation. In the fabrication of the model, primary importance had been placed on weight and strength constraints, rather than on duplicating mass and inertia effects. One result was a mass imbalance in the stabilators in which the center-of-gravity-location was 4.4 centimeters rearward of the hinge line.

When the low-pass filters were added to the rate damper mode, the 10-hertz oscillation did not occur until a gain of 3.0 seconds was used. This was 7.5 times the maximum gain selected for flight (table 2). A similar resonance was observed in testing the pitch CAS mode. The pitch rate CAS feedback excited a structural instability at approximately 20 hertz at a gain of 4.0 deg/g with no notch filtering on pitch rate or normal acceleration. When the notch filters were added, the 10-hertz oscillation was again observed at a gain of 4.0 deg/g. This gain is four times the pitch CAS gain (table 2).

No structural resonances were observed for the roll and yaw rate damper and CAS modes, although the roll rate damper mode did excite the tail-wags-dog oscillation at a gain of 4.0 seconds with the notch and low-pass filters. Again, this was five times the roll CAS gain (table 2). Thus the ground resonance checks established stability margins for all axes of the rate damper and CAS modes. A minimum stability margin of 12 decibels was verified for the pitch, roll, and yaw axes of the two augmented modes.

FLIGHT-TEST RESULTS

Before the scale-model F-15 was air launched, two captive flights were made to check the operation of the telemetry links, onboard systems, and RPRV facility. Data from the first nine drop flights are presented in this section. Additional data from the first four flights are presented in reference 3.

The flight program was scheduled so that the modes and components of the RPRV/RAV system could be activated gradually. Thus the remotely augmented rate damper and CAS modes were not activated until the open-loop operation of the system had

been demonstrated. The early flights were devoted largely to obtaining basic stability and control data to verify the wind-tunnel data used in the simulation. These manuevers were performed using the computer direct and rate damper modes. After these stability and control flights were made, the model was flown in the MCS and CAS modes, and aggravated inputs were applied to investigate its stall, departure, and spin characteristics.

Basic Modes

The computer direct and rate damper modes were designed to permit the pilot to perform stability and control maneuvers efficiently. In the nine flights of the model (40 minutes of flight time), approximately 100 stability and control maneuvers have been performed using these control modes.

The unaugmented modes were used on the first flight of the model, and data were obtained from $\alpha = 5°$ to $26°$. Simulation studies had indicated very light damping of the Dutch roll and short-period modes, so use of the rate damper mode was planned for subsequent flights. Power spectra were obtained from the first flight for roll, pitch, and yaw rates and normal and lateral accelerations at several angles of attack. All the variables showed a strong resonance at approximately 20 hertz; the intensity of the resonance was a function of angle of attack. At $\alpha < 10°$ all the signals were clean, with the accelerations indicating a broad low-amplitude resonance of approximately 50 hertz. Above $\alpha = 10°$ the energy at approximately 20 hertz increased with angle of attack on all signals until an angle of attack of $20°$ was reached, after which it remained constant. The resonance may have been caused by buffet characterized by locally separated flow on the wing at high angles of attack which excited the approximately 20-hertz structural modes.

Before using the rate damper or CAS modes, it was necessary to consider the possibility of closed-loop structural resonance. The versatility of the RPRV computer permitted a simple solution to this problem: the implementation of digital notch filters in the control law computation.

The power spectra from the first flight were used to select frequencies for notch filters on roll, pitch, and yaw rates and normal and lateral accelerations. Five notch filters were added to the program between the first two drop flights. In addition, 6-hertz low-pass filters were applied to the roll, pitch, and yaw rates for the rate damper mode to aid in the attenuation of high-frequency structural resonances. The filter used to simulate the F-15 series servos performed a similar high-frequency attenuation in the CAS mode.

The rate damper mode was activated on the third flight and operated as expected. The operation of the pitch and the roll and yaw dampers is shown in figure 24. Figure 24(a) shows the open-loop pitch response to a stabilator doublet followed by the operation of the pitch damper after several oscillations. The pitch damper was effective in damping the short-period mode of the vehicle, as had been predicted. Figure 24(b) shows the operation of the roll and yaw rate dampers at angles of attack of $28°$ to $31°$. Three successive open-loop manuevers are shown with the damper system operating between maneuvers. During the maneuvers, the model is excited by aileron, rudder, and differential stabilator doublets. The doublets are indicated

36
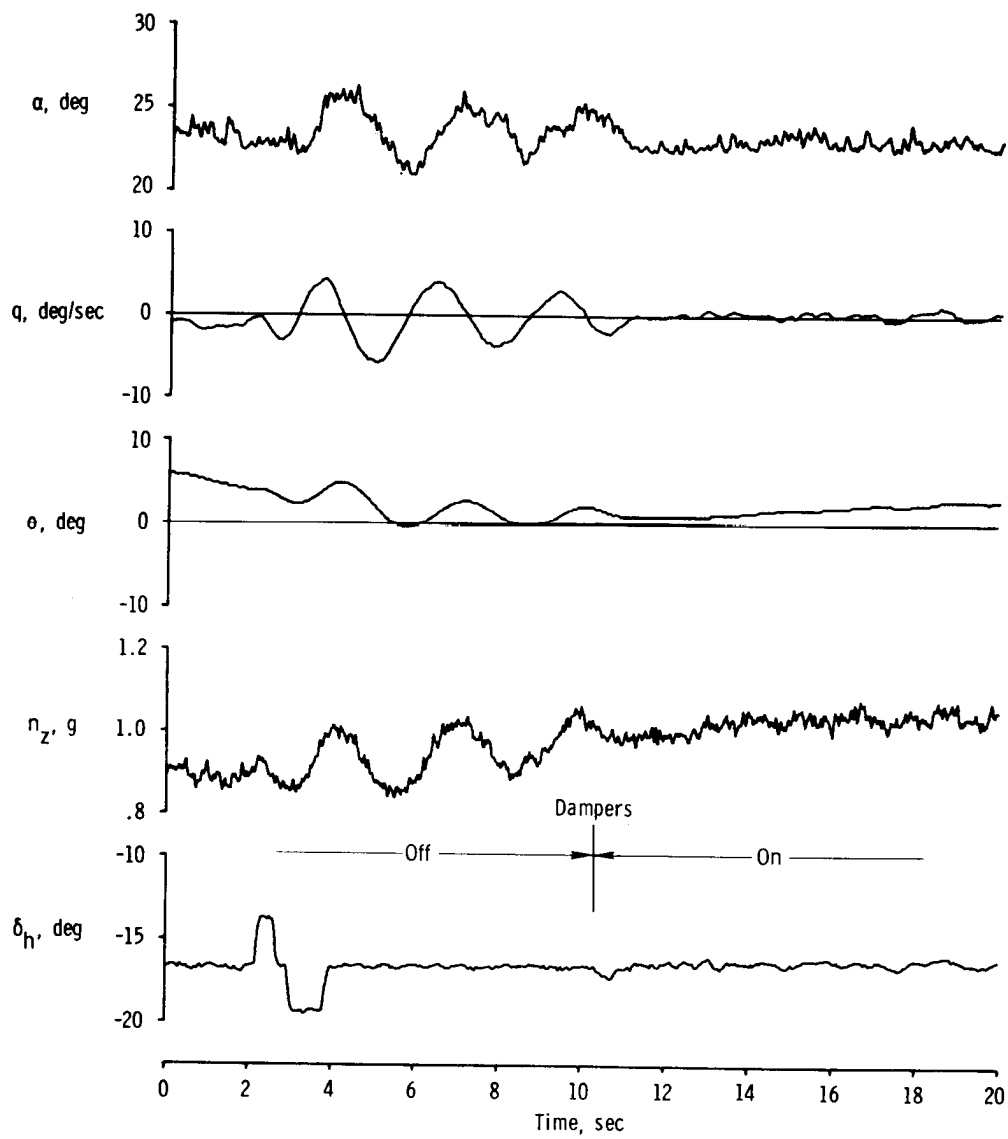
(a)   Pitch rate damper, $K_q = 0.4$ sec.

Figure 24.   Operation of rate damper system.
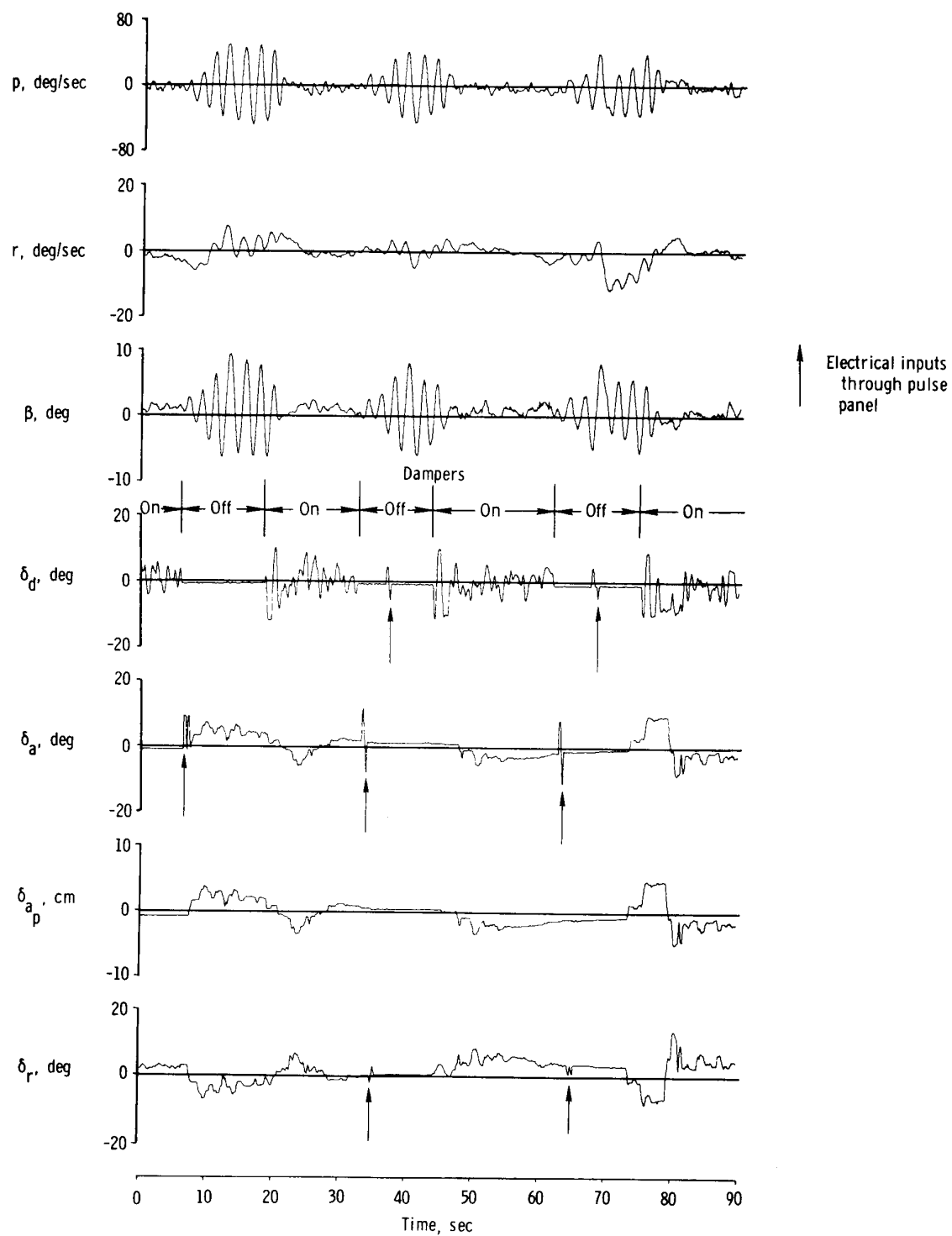
(b) *Roll and yaw rate dampers*, $\alpha = 28°$ to $31°$, $K_p = -0.8$ sec, $K_r = 1.0$ sec.

Figure 24. Concluded.

38

by arrows on the δ_d, δ_a, and δ_r traces and were commanded electrically through the pulse panel. The pilot did not use the rudder pedals; all rudder motion is due to the aileron-to-rudder interconnect, the yaw damper, and the pulse panel inputs. The figure shows that the open-loop airplane's Dutch roll mode at this angle of attack was unstable for small oscillations in p, r, and β and that the dampers were effective in damping the oscillations.

The RPRV computer program was modified and recompiled between each flight. Most of the changes were associated with the computer direct and rate damper modes and were implemented to help the pilot obtain high-quality stability and control data. Stability and control derivatives have been identified over a range of angle of attack from -20° to 40°. Changes were made in the damper gain, control authority (for example, lateral stick gearing), and pulse panel software. Also, the aileron-to-rudder interconnect was incorporated to aid in turn coordination. To obtain the negative-angle-of-attack data, the model was flown inverted for prolonged periods and trimmed with forward stick inputs. No difficulty was experienced with the telemetry links in these maneuvers.

In preparation for the CAS flight tests, several maneuvers were performed in the basic modes at stick deflections equal to the maximum stabilator authority in CAS. For example, on the fourth flight the model was trimmed at $\alpha = 31°$ and flown in the computer direct mode with full aft stick ($\delta_h = -27.5°$), which is the maximum stabilator authority of the full-scale F-15 CAS mode. On the seventh flight, with the center of gravity at 30-percent mean aerodynamic chord, the model was trimmed at $\alpha = 40°$ with full aft stick.

F-15 Control System Modes

The MCS and CAS modes were fully exercised during the nine flights of the model. The MCS mode was used on every flight. The first five flights were flown with the center of gravity at the 26-percent mean aerodynamic chord location, and the following four flights at the 30-percent mean aerodynamic chord location. On the second flight the model was flown for several minutes in the MCS mode with full aft longitudinal stick ($\delta_h = 23°$) and trimmed at $\alpha = 28°$.

The CAS mode was used for the first time on the fifth flight and operated as expected. No problems were encountered in the use of acceleration feedbacks in the pitch and yaw axes. Figure 25 shows the model's pitch CAS response to pilot input during flight and in the RPRV digital simulation. The closed-loop bandwidth of the pitch CAS is approximately 4 radians per second. The pilot's input was the same as that in figure 23. Figure 25 shows good correlation between the flight and simulation responses.

Complete verification that the model F-15 under control of the digital RAV system in flight provides a valid scaled simulation of the full-scale F-15 airplane with onboard analog control system would entail a number of steps and require flight data from the full-scale F-15 airplane. Full-scale F-15 flight data were not available;
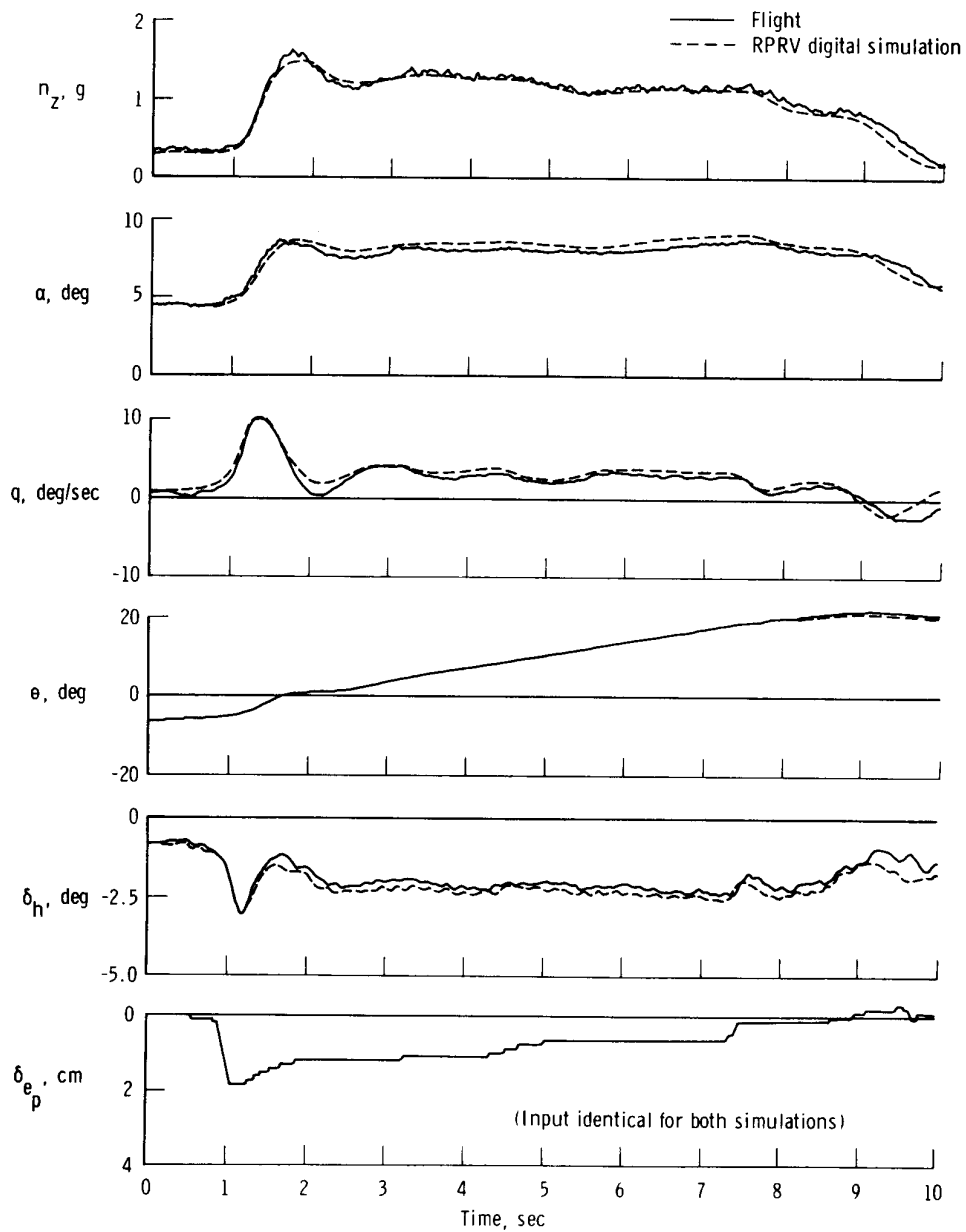
Figure 25. Comparison of pitch CAS response to pilot input during flight and in RPRV digital simulation.

however, most of the key steps were taken to verify the technique. The RPRV digital simulation was validated as an accurate simulation of the closed-loop model F-15 in flight (fig. 25) and then compared with the analog CAS simulation (fig. 23). Since both figures show close agreement in vehicle motion response for identical inputs and initial conditions, the assumption that the digital RAV system in control of the model F-15 in flight would provide a valid simulation of an onboard analog system in control of the same model can be made with confidence.

High-angle-of-attack stall and spin departure studies were started on the third flight, utilizing the MCS mode. Aggravated inputs (full aft and full lateral stick) were applied in this mode on the third and fourth flights, but no control problems were experienced. On the fifth flight, using the additional control surface authority provided by the CAS mode, attempts to spin the model were again unsuccessful. A spin was finally achieved on the seventh flight by using a spin entry control scheme developed on the simulation. The model recovered easily when spin recovery controls were applied. Two more spins were performed on the following flight, and again no difficulty was experienced in recovering. As noted previously, the stall inhibiter function of the full-scale F-15 CAS was not implemented in the RPRV computer program for these tests. The spin entries were started with the computer in the CAS mode, and the computer automatically downmoded to the MCS on each spin entry when the yaw rate exceeded 70 degrees per second.

The results of this series of flights, which involved high-risk flight testing and the use of the remote augmentation system to perform the control function, demonstrate the usefulness of the RPRV system. An approach this aggressive would not usually be attempted in a manned program.

RPRV FACILITY OPERATIONAL EXPERIENCE

The operation of the RPRV system during the first nine flights of the scale-model F-15 showed that the RPRV approach to flight testing is a promising method for advanced systems testing and hazardous flight testing. The remote augmentation system, which utilizes a ground-based computer, did not experience a failure during flight; however, problems did occur with the telemetry downlink and uplink.

On the second flight, the ground station receiver was slightly out of adjustment, which made the remote pilot's displays unusable because of downlink dropout. This adjustment was carefully monitored during the following flights, and the problem did not recur. No other downlink dropout was experienced during the test time on any of the other flights.

The uplink command system functioned perfectly during the first five flights; however, a problem which occurred during attempts to make the sixth flight resulted in two aborted flights. On both of the aborted flights and on the sixth flight, the uplink signal strength dropped below a preset threshold. Proper action was taken by the system in each instance: On the aborted flights a low signal level was indicated, and on the sixth flight the onboard autopilot system was activated. The difficulty

was traced to a series of unrelated alinement and calibration problems. The most important of these was faulty boresighting of the uplink system ground antenna. Modifications were made to the onboard receiver to permit the signal strength level to be monitored through the telemetry downlink. After the system was properly alined and calibrated, three additional flights were made without incident.

The RPRV system operation has also provided information about the capability of a remote pilot to control a vehicle during unrestricted maneuvering. The F-15 model was flown through an extensive range of attitudes, including 360° rolls and 90° nose-down attitudes. High oscillatory rates of 200 deg/sec in roll, 100 deg/sec in pitch, and 200 deg/sec in yaw were sustained, and the model experienced elevated acceleration maneuvers up to its structural design limit (4g). As noted, the model was flown in an inverted attitude for prolonged periods to obtain data at negative angles of attack, and aggravated full authority control inputs in both the MCS and CAS modes were made in attempts to force the model into departures and spins.

The interaction between the remote pilot and the RPRV systems proved to be of great benefit in accomplishing the research objectives of the program. By utilizing the flight planning simulator and the control of the RPRV computer software afforded by the mode control panel and the pulse panel, the pilot was able to perform many high-quality stability and control maneuvers. The FORTRAN programing capability made it possible for suggestions by the pilot or required additions to the software to be implemented quickly and made available for the next flight. For example, it was necessary to add five notch filters and three low-pass filters in the rate damper mode to the computer program between the first and second flights. This was accomplished easily within the planned 1½ weeks between the flights. Also, it was necessary to modify the scale-model F-15 modes in order to duplicate modifications made in the full-scale F-15 flight control system during its initial flight testing. These modifications were made easily in the RPRV computer software.

The RPRV system operation was enhanced by the use of floating point FORTRAN coding to write the RPRV computer programs. This capability was in keeping with the overall philosophy of low-cost subscale testing, in that the control system engineer was able to write the flight control system software directly. He thus had direct control of the software and could use the FORTRAN compiler to check out and debug the program. The ability to run the identical program card deck in the RPRV digital simulation was a further check on the software.

CONCLUDING REMARKS

The remote augmentation capability of the remotely piloted research vehicle (RPRV) facility at the NASA Flight Research Center was used in flight tests of a 3/8-scale model of the F-15 airplane. It was found that coupling the remote piloting task with the remote augmentation technique in a ground-based digital computer made it possible to achieve the research objectives of the subscale F-15 program. The use of FORTRAN programing made it easy to write and modify the program containing the control laws.

42

The validity of the remote augmentation concept of implementing closed-loop feedback control of a remotely piloted research vehicle in a ground-based digital computer was demonstrated. Rate damper and control augmentation systems were successfully implemented for the scale model.

The integrity of the RPRV facility's uplink and downlink telemetry systems was demonstrated for the control and remote augmentation of unmanned models. The telemetry links operated for extended periods and over an extensive range of vehicle attitudes without transmission difficulties.

The remote augmentation technique of simulating an analog flight control system was successful. The RPRV system accurately simulated the F-15 analog control augmentation system.

Flight Research Center
  National Aeronautics and Space Administration
    Edwards, Calif., January 6, 1975

43

APPENDIX A

MODEL SCALING TECHNIQUES

Scale-model flight testing requires an understanding of the scaling laws that relate the dynamic behavior of the scale model to that of the full-scale aircraft. It is important to realize that exact similitude between the model and the full-scale airplane cannot be achieved, and that a choice must be made between several available scaling techniques. Also, in designing remote augmentation systems for use with scale models, it is necessary to compensate for scaling effects in the closed-loop control laws by modifying feedback gains.

Figure A1 shows the forces, moments, and geometry relevant to the dynamic response of a model and a full-scale airplane. The functional dependencies of the forces and moments are indicated in the figure. Table A1 lists the scaling relationships which would have to be satisfied for exact similitude. Relation 1 is a statement of the model scale factor, and relation 2 is a statement of the requirement of matching helix angles so that the vehicles follow geometrically similar flightpaths. There are eight relations between the seven variables: model scale factor, a, frequency, ω, velocity, V, Mach number, M, mass, m, moment of inertia, I, and atmospheric density, ρ. Thus, in general, at least one of the relations will not be satisfied. The relations chosen to be matched are determined by the purpose of the scale-model test.
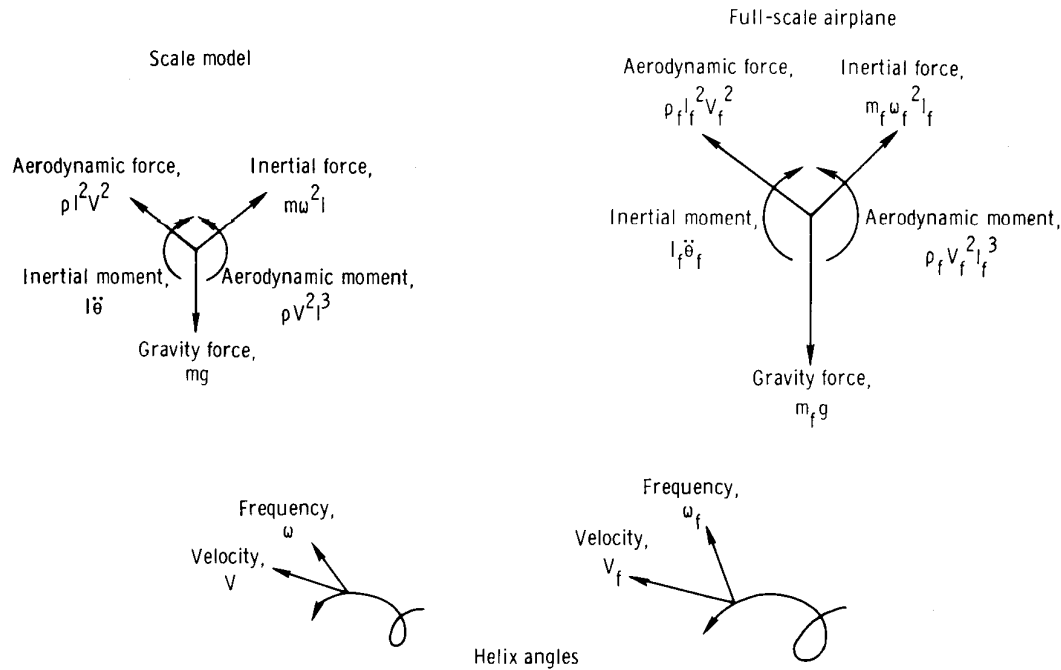

Figure A1. Force, moment, and helix diagrams of scale model and full-scale airplane.

44

TABLE A1.— SCALING RELATIONSHIPS IN MODEL TESTING

Relation	Quantity
1 $\quad l = al_f$	Length
2 $\quad \dfrac{\omega l}{V} = \dfrac{\omega_f l_f}{V_f}$	Helix angle
3 $\quad \dfrac{V}{V_c} = \dfrac{V_f}{V_{c_f}}$	Mach number $\left(M = \dfrac{V}{V_c} \right)$
4 $\quad \dfrac{Vl}{\nu} = \dfrac{V_f l_f}{\nu_f}$	Reynolds number
5 $\quad \dfrac{I\ddot{\theta}}{\rho l^3 V^2} = \dfrac{I_f \ddot{\theta}_f}{\rho_f l_f^3 V_f^2}$	Ratio of inertial moments to aerodynamic moments
6 $\quad \dfrac{m\omega^2 l}{\rho l^2 V^2} = \dfrac{m_f \omega_f^2 l_f}{\rho_f l_f^2 V_f^2}$	Ratio of inertial forces to aerodynamic forces
7 $\quad \dfrac{m}{m\omega^2 l} = \dfrac{m_f}{m_f \omega_f^2 l_f}$	Ratio of gravitational forces to inertial forces
8 $\quad \dfrac{m}{\rho l^2 V^2} = \dfrac{m_f}{\rho_f l_f^2 V_f^2}$	Ratio of gravitational forces to aerodynamic forces

For wind-tunnel testing, the length, Reynolds number, and Mach number relations are usually matched (refs. 7 and 8). For free-flight model testing, scaling relationships must be chosen on the basis of the dynamic pressure region being investigated. If compressibility effects are being investigated, the Mach number is matched (ref. 9). For dynamic testing at low dynamic pressures, the Froude number (ratio of inertial forces to gravitational forces) is held invariant (ref. 10). This inertia-gravity scaling technique was used for the scale-model F-15.

Requiring that the ratio of inertial forces to gravitational forces be held invariant while at the same time matching helix angles places a constraint upon the model velocity (relations 2 and 7, table A1). This constraint may be stated in the form of a scaling law, $V = a^{\frac{1}{2}}V_f$. The remaining relations between forces and moments (relations 5, 6, and 8) are matched by properly scaling the model's mass and inertias. Table A2 lists the complete set of scaling laws for an invariant inertia-gravity relationship. Note that mass and inertia scaling is a function of the ratio of atmospheric pressures, ρ/ρ_f. Proper selection of model altitude provides some independent control over these scaling ratios.

TABLE A2.— SCALING LAWS FOR INVARIANT
INERTIA-GRAVITY RELATIONSHIP

Quantity	Scale factor
Model scale	a
Density	$\dfrac{\rho}{\rho_f}$
Mass	$a^3\dfrac{\rho}{\rho_f}$
Inertia	$a^5\dfrac{\rho}{\rho_f}$
Mach number	$a^{\frac{1}{2}}\dfrac{V_c}{V_{c_f}}$
Velocity	$a^{\frac{1}{2}}$
Linear acceleration	1
Angles	1
Angular velocity	$a^{-\frac{1}{2}}$
Angular acceleration	a^{-1}
Time	$a^{\frac{1}{2}}$
Reynolds number	$a^{\frac{3}{2}}\dfrac{\nu}{\nu_f}$

The scaling indicated in table A2 is particularly important in interpreting a scale model's dynamic response and the effect of scaling on closed-loop model operation. Using two-degree-of-freedom longitudinal equations of motion, reference 11 derives the short-period natural frequency and damping as

$$\omega_{sp} = \sqrt{M_q Z_\alpha - M_\alpha} \qquad (A1)$$

$$\zeta_{sp} = \frac{-\left(Z_\alpha + M_q\right)}{2\omega_{sp}} \qquad (A2)$$

Because the model is scaled to be geometrically similar to the full-scale airplane, the nondimensional stability derivatives of the two vehicles will be the same. Dimensionalizing the derivatives (as shown in ref. 11) at the same altitude and using the inertia-gravity scaling laws of table A2 gives the following relationship between model and full-scale dimensionalized derivatives:

$$Z_\alpha = a^{-\frac{1}{2}} Z_{\alpha_f}$$

$$Z_{\delta_e} = a^{-\frac{1}{2}} Z_{\delta_{e_f}}$$

$$M_\alpha = a^{-1} M_{\alpha_f}$$

$$M_q = a^{-\frac{1}{2}} M_{q_f}$$

$$M_{\delta_e} = a^{-1} M_{\delta_{e_f}}$$

Substitution in equations (A1) and (A2) gives

$$\omega_{sp} = a^{-\frac{1}{2}} \omega_{sp_f} \qquad (A3)$$

$$\zeta_{sp} = \zeta_{sp_f} \qquad (A4)$$

Thus the frequencies of the response modes of the model are increased by $a^{-\frac{1}{2}}$ over those of the full-scale vehicle, whereas the damping ratios are unchanged. This reflects the time scaling indicated in table A2.

For closed-loop control of scale models the airplane response is modified; however, it is necessary that the scaling relations of equations (A3) and (A4) hold for the

closed-loop vehicle as well. To investigate the effect of scaling on the control system, the following general feedback control law is postulated:

$$\delta_h = K_\theta \theta + K_\alpha \alpha + K_q q + K_{n_z} n_z$$

When this general control law is substituted into the two-degree-of-freedom short-period mode approximation equations of reference 12 and the scaling laws of table A2 are applied, the closed-loop frequency and damping of the model will obey equations (A3) and (A4) if only the pitch rate feedback gain is scaled as

$$K_q = a^{\frac{1}{2}} K_{q_f}$$

None of the other feedback gains require scaling. In general, all angular rate feedback gains of the full-scale airplane must be reduced by the square root of the scaling ratio. Also, the critical frequencies of control system components such as shaping filters and actuators must be increased as in equation (A3). The critical parameters of nonlinear components must be adjusted according to the appropriate scaling law, as well. For example, angular rate limits must be increased by $a^{-\frac{1}{2}}$, corresponding to the angular velocity scale factor in table A2.

DIGITAL FILTERING TECHNIQUE

To utilize the RPRV system, the systems engineer must use digital filtering techniques to simulate analog systems, implement digital control systems, and suppress undesirable noise and structural resonances in the test vehicle's response signals. The problem of shaping the frequency content of a continuous signal with linear analog filters is well understood, and it is desirable to use this knowledge in designing digital filters. The resulting problem is that of approximating the filtering action of a continuous linear filter on a continuous waveform with a linear digital filter operating on a sampled continuous waveform. Many techniques are available, among them numerical integration and the standard z-transform. Numerical integration techniques are usually inefficient for real-time operations because they rely on repeated evaluations of functions to produce a solution and they do not take advantage of the known structure of linear filters. The standard z-transform technique is the natural choice for analyzing discrete system stability, but it has drawbacks when used for approximating continuous transfer functions (ref. 5). Two of these drawbacks are the aliasing of power about the Nyquist frequency and the difficulty of implementing some standard filter forms such as high-pass filters.

The derivation of the filtering algorithm used in the RPRV computer program is illustrated in figure B1. The poles and zeros of the continuous transfer function
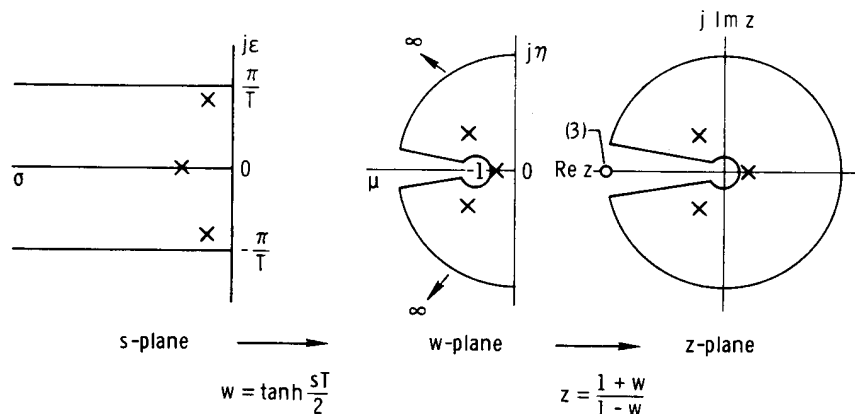

$$w = \tanh \frac{sT}{2}$$

$$z = \frac{1 + w}{1 - w}$$

Figure B1. Conformal mappings between the s-, w-, and z-planes used in defining the digital filtering algorithm for the RPRV computer program.

$G(s)$ contained in the primary strip of the s-plane are mapped into the left half of the intermediate w-plane by means of the complex transformation

$$w = \tanh \frac{sT}{2}$$

The transformation maps a root located at $s = \sigma + j\varepsilon$ to a root located at $w = \mu + j\eta$ with

$$\mu = \frac{\sinh \sigma T}{\cosh \sigma T + \cos \varepsilon T}$$

$$\eta = \frac{\sin \varepsilon T}{\cosh \sigma T + \cos \varepsilon T}$$

Note that the imaginary s-plane axis from $-\frac{\pi}{T}$ to $\frac{\pi}{T}$ maps onto the entire imaginary axis of the w-plane. The negative real axis in the s-plane maps onto the negative segment of the real axis of the w-plane from -1 to 0. The final step of the algorithm maps the function $G(w)$ into the unit circle of the z-plane through the bilinear transformation

$$z = \frac{1 + w}{1 - w}$$

The transformation maps a root located at $w = \mu + j\eta$ to a root located at $z = Re\ z + j\ Im\ z$:

$$Re\ z = \frac{1 - \mu^2 + \eta^2}{(1 - \mu)^2 + \eta^2}$$

$$Im\ z = \frac{2\eta}{(1 - \mu)^2 + \eta^2}$$

It can be shown that the complete algorithm maps roots from the s-plane to the z-plane such that a real root located at $s = -\beta$ will map to a real root located at $z = e^{-\beta T}$, and a pair of complex conjugate roots with the characteristic polynomial $(s + c)^2 + d^2$ will map to a pair of complex conjugate roots with the characteristic polynomial $z^2 - 2e^{-cT} \cos dT\ z + e^{-2cT}$. Band-limited transforms, such as low-pass filters, with more poles than zeros have additional zeros inserted at $z = -1$ such that the orders of the denominator and the numerator of $G(z)$ are the same. The effect of these zeros at $z = -1$ (for low-pass filter forms) is to introduce a "notch" characteristic in the frequency response of the digital filter at the half-sample frequency. This is in addition to the desired low-pass characteristic for which the filter was designed and may be regarded as a "free" noise rejection capability of the digital filter at frequencies near the half-sample frequency.

The complete algorithm can be stated as follows: Given a continuous transfer function,

$$G(s) = \frac{K' \prod\limits_{i=1}^{u}\left(s + \alpha_i\right)\prod\limits_{i=1}^{n}\left[\left(s + a_i\right)^2 + b_i^2\right]}{\prod\limits_{i=1}^{r}\left(s + \beta_i\right)\prod\limits_{i=1}^{t}\left[\left(s + c_i\right)^2 + d_i^2\right]}$$

a digital filter approximating $G(s)$ is given by

$$G(z) = \frac{K''(z + 1)^k \prod\limits_{i=1}^{u}\left(z - e^{-\alpha_i T}\right)\prod\limits_{i=1}^{n}\left(z^2 - 2e^{-a_i T}\cos b_i Tz + e^{-2a_i T}\right)}{\prod\limits_{i=1}^{r}\left(z - e^{-\beta_i T}\right)\prod\limits_{i=1}^{t}\left(z^2 - 2e^{-c_i T}\cos d_i Tz + e^{-2c_i T}\right)} \qquad \text{(B1)}$$

where $k = r + 2t - u - 2n$, $k \geq 0$, and K'' is the normalization constant. For unity gain low-pass filters, K'' is set by the condition $G(z)\Big|_{z=+1} = 1$, and for unity gain high-pass filters, by the condition $G(z)\Big|_{z=-1} = 1$.

The preceding digital filtering algorithm is an extension of algorithms described by Kaiser in reference 5 and Gold and Rader in reference 4. The algorithms discussed in these references are referred to as the bilinear transformation, although the algorithms are not the same. The algorithm described by Kaiser is also known as Tustin's method and involves trapezoidal integration of the differential equation describing the continuous transfer function. The algorithm described by Gold and Rader performs a prewarping of the critical frequencies of the filter transfer function before the application of the bilinear transformation. In both of these algorithms, the root locations of the resulting digital filters are approximations to those given by equation (B1). The matched z-transform algorithm (ref. 12) gives the same pole and zero locations as equation (B1) but does not account for the zeros added at $z = -1$ for band-limited functions. In the use of the matched z-transform, it is common to add these zeros in an *ad hoc* manner.

REFERENCES

1. Edwards, John W.: Flight-Test of a Remotely Piloted Research Vehicle Using a Remote Digital Computer for Control Augmentation. Transactions of the First NWC Symposium on the Application of Control Theory to Modern Weapons Systems - 9-10 May 1973. NWC TP 5522, Naval Weapons Center (China Lake, Calif.), June 1973, pp. 281-308.

2. Reed, R. Dale: RPRVs - The First and Future Flights. Astronaut. Aeron., Apr. 1974, pp. 26-42.

3. Holleman, Euclid C., compiler: Initial Results From Flight Testing a Large, Remotely Piloted Airplane Model. NASA TM X-56024, 1974.

4. Gold, Bernard; and Rader, Charles M.: Digital Processing of Signals. McGraw-Hill Book Co., Inc., c.1969, pp. 48-97.

5. Kaiser, J. F.: Digital Filters. Ch. 7 of Systems Analysis by Digital Computer, Franklin F. Kuo and James F. Kaiser, eds., John Wiley & Sons, Inc., c.1966, pp. 218-285.

6. Tobie, Harold N.; Malcom, Lawrence G.; and Elliott, Elden M.: A New Longitudinal Handling Qualities Criterion. NAECON/66; Proceedings of the IEEE 18th Annual National Aerospace Electronics Conference, May 1966, pp. 93-99.

7. Shapiro, Ascher H.: The Dynamics and Thermodynamics of Compressible Fluid Flow. Vol. I. The Ronald Press Co., c.1953, p. 56.

8. Kuethe, A. M.; and Schetzer, J. D.: Foundations of Aerodynamics. 2nd ed., John Wiley & Sons, Inc., c.1959, pp. 11, 243-244, 260-261.

9. Neihouse, Anshal I.; and Pepoon, Philip W.: Dynamic Similitude Between a Model and a Full-Scale Body for Model Investigation at Full-Scale Mach Number. NACA TN 2062, 1950.

10. Scherberg, Max; and Rhode, R. V.: Mass Distribution and Performance of Free Flight Models. NACA TN 268, 1927.

11. Northrop Servomechanisms Section and Aerodynamics Section: Dynamics of the Airframe. AE-61-4II, Bur. of Aeron., Navy Dept., Sept. 1952, pp. II-29 - III-7. (Available from Northrop Corp., Norair Div.)

12. Slater, G. L.: A Unified Approach to Digital Flight Control Algorithms. AIAA Paper No. 74-884, Aug. 1974.